

Loss of Mitochondrial Ca²⁺ Uniporter Limits Inotropic Reserve and Provides Trigger and Substrate for Arrhythmias in Barth Syndrome Cardiomyopathy

Running title: *Bertero et al.; Mechano-energetic Uncoupling in Barth Syndrome*

Edoardo Bertero, MD^{1,2}; Alexander Nickel, PhD¹; Michael Kohlhaas, PhD¹; Mathias Hohl, PhD³; Vasco Sequeira, PhD¹; Carolin Brune, MD³; Julia Schwemmlin, BSc¹; Marco Abeßer, BS⁴, Kai Schuh, PhD⁴; Ilona Kutschka, MSc¹; Christopher Carlein, BSc⁵; Kai Münker, MD^{1,3}; Sarah Atighetchi, MD^{1,3}; Andreas Müller, PhD⁶; Andrey Kazakov, PhD³; Reinhard Kappl, PhD⁵; Karina von der Malsburg, PhD⁷; Martin van der Laan, PhD⁷; Anna-Florentine Schiuma, BSc¹; Michael Böhm, MD³; Ulrich Laufs, MD^{3,8}; Markus Hoth, PhD⁵; Peter Rehling, PhD^{9,10,11}; Michaela Kuhn, MD⁴; Jan Dudek, PhD^{1,9}; Alexander von der Malsburg, PhD⁷; Leticia Prates Roma, PhD⁵; Christoph Maack, MD^{1,3*,12}

¹Department of Translational Research, Comprehensive Heart Failure Center, University Clinic Würzburg, Germany; ²Chair of Cardiovascular Disease, Department of Internal Medicine and Specialties (Di.M.I.), University of Genoa, Italy (current address); ³Clinic for Internal Medicine III, Saarland University Clinic, Homburg/Saar, Germany; ⁴Institute of Physiology, University of Würzburg, Würzburg, Germany; ⁵Department for Biophysics, ZHMB, CIPMM, Saarland University, Homburg/Saar, Germany; ⁶Clinic for Radiology, Saarland University Clinic, Homburg/Saar, Germany; ⁷Medical Biochemistry and Molecular Biology, Center for Molecular Signaling, PZMS, Faculty of Medicine, Saarland University, Homburg/Saar, Germany; ⁸Klinik und Poliklinik für Kardiologie, Universitätsklinikum Leipzig, Germany (current address); ⁹Department of Cellular Biochemistry, Georg-August University, Göttingen, Germany; ¹⁰Cluster of Excellence "Multiscale Bioimaging: from Molecular Machines to Networks of Excitable Cells" (MBExC), University of Göttingen, Germany; ¹¹Max-Planck Institute for Biophysical Chemistry, D-37077, Göttingen, German; ¹²Department for Internal Medicine 1, University Clinic Würzburg, Germany

Address of correspondence:

Christoph Maack, MD
Comprehensive Heart Failure Center (CHFC)
University Clinic Würzburg
Am Schwarzenberg 15, Haus A15
97078 Würzburg
Germany
Maack_C@ukw.de
Tel.: +49-931-201-46502
Fax: +49-931-201-646502

*This article is published in its accepted form, it has not been copyedited and has not appeared in an issue of the journal. Preparation for inclusion in an issue of *Circulation* involves copyediting, typesetting, proofreading, and author review, which may lead to differences between this accepted version of the manuscript and the final, published version.

Abstract

Background: Barth syndrome (BTHS) is caused by mutations of the gene encoding tafazzin, which catalyzes maturation of mitochondrial cardiolipin and often manifests with systolic dysfunction during early infancy. Beyond the first months of life, BTHS cardiomyopathy typically transitions to a phenotype of diastolic dysfunction with preserved ejection fraction, blunted contractile reserve during exercise and arrhythmic vulnerability. Previous studies traced BTHS cardiomyopathy to mitochondrial formation of reactive oxygen species (ROS). Since mitochondrial function and ROS formation are regulated by excitation-contraction (EC) coupling, integrated analysis of mechano-energetic coupling is required to delineate the pathomechanisms of BTHS cardiomyopathy.

Methods: We analyzed cardiac function and structure in a mouse model with global knockdown of tafazzin (*Taz*-KD) compared to wild-type (WT) littermates. Respiratory chain assembly and function, ROS emission, and Ca^{2+} uptake were determined in isolated mitochondria. EC coupling was integrated with mitochondrial redox state, ROS, and Ca^{2+} uptake in isolated, unloaded or preloaded cardiac myocytes, and cardiac hemodynamics analyzed *in vivo*.

Results: *Taz*-KD mice develop heart failure with preserved ejection fraction (>50%) and age-dependent progression of diastolic dysfunction in the absence of fibrosis. Increased myofilament Ca^{2+} affinity and slowed cross-bridge cycling caused diastolic dysfunction, partly compensated by accelerated diastolic Ca^{2+} decay through preactivated sarcoplasmic reticulum Ca^{2+} ATPase (SERCA). *Taz* deficiency provoked heart-specific loss of mitochondrial Ca^{2+} uniporter (MCU) protein that prevented Ca^{2+} -induced activation of the Krebs cycle during β -adrenergic stimulation, oxidizing pyridine nucleotides and triggering arrhythmias in cardiac myocytes. *In vivo*, *Taz*-KD mice displayed prolonged QRS duration as a substrate for arrhythmias, and a lack of inotropic response to β -adrenergic stimulation. Cellular arrhythmias and QRS prolongation, but not the defective inotropic reserve, were restored by inhibiting Ca^{2+} export via the mitochondrial $\text{Na}^+/\text{Ca}^{2+}$ exchanger. All alterations occurred in the absence of excess mitochondrial ROS *in vitro* or *in vivo*.

Conclusions: Downregulation of MCU, increased myofilament Ca^{2+} affinity, and preactivated SERCA provoke mechano-energetic uncoupling that explains diastolic dysfunction and the lack of inotropic reserve in BTHS cardiomyopathy. Furthermore, defective mitochondrial Ca^{2+} uptake provides a trigger and a substrate for ventricular arrhythmias. These insights can guide the ongoing search for a cure of this orphaned disease.

Key Words: Barth syndrome; mitochondria; mitochondrial calcium uniporter; mitochondrial redox state; oxidative stress; excitation-contraction coupling.

Non-standard abbreviations and acronyms

ADP, adenosine diphosphate; ATP, adenosine triphosphate; BTHS, Barth syndrome; $[\text{Ca}^{2+}]_c$, cytosolic Ca^{2+} concentration; CaMKII, Ca^{2+} /calmodulin-dependent protein kinase II; CL, cardiolipin; DCM, dilated cardiomyopathy; EC coupling, excitation-contraction coupling; ETC, electron transport chain; GPX1, glutathione peroxidase 1; HCM, hypertrophic cardiomyopathy; HFpEF/HFrEF, heart failure with preserved/reduced ejection fraction; IMM, inner mitochondrial membrane; iPSC, inducible pluripotent stem cell; Iso, isoproterenol; K_{ATP} , sarcolemmal ATP-dependent K^+ channels; LV, left

ventricle; LVEF, left ventricular ejection fraction; MCU, mitochondrial Ca^{2+} uniporter; NCX, sarcolemmal $\text{Na}^+/\text{Ca}^{2+}$ exchanger; NCLX, mitochondrial $\text{Na}^+/\text{Ca}^{2+}$ exchanger; NNT, nicotinamide nucleotide transhydrogenase; PKA, protein kinase A; PLN, phospholamban; PRDX, peroxiredoxin; PTP, permeability transition pore; ROS, reactive oxygen species; SOD, superoxide dismutase; SERCA, SR Ca^{2+} ATPase; SR, sarcoplasmic reticulum; *Taz*, tafazzin gene.



Circulation

Clinical perspective

What is new?

- Barth syndrome cardiomyopathy in tafazzin-knockdown mice is characterized by early and progressive diastolic dysfunction induced by slowed cross-bridge cycling and increased myofilament Ca^{2+} sensitivity
- The inherited defect in cardiolipin remodeling leads to loss of mitochondrial Ca^{2+} uniporter protein in cardiac, but not skeletal muscle
- Defective mitochondrial Ca^{2+} uptake prevents Krebs cycle activation during β -adrenergic stimulation, abolishes NADH regeneration for ATP production and lowers antioxidative NADPH
- Mitochondrial Ca^{2+} deficiency provides trigger and substrate for ventricular arrhythmias and contributes to blunted inotropic reserve during β -adrenergic stimulation
- These changes occur without any increase of reactive oxygen species formation in- or emission from mitochondria

What are the clinical implications?

- Beyond the first months of life, when systolic dysfunction dominates, Barth syndrome cardiomyopathy is reminiscent of heart failure with preserved rather than reduced ejection fraction, presenting with progressive diastolic and moderate systolic dysfunction without relevant left ventricular dilation
- Defective mitochondrial Ca^{2+} uptake contributes to inability of Barth syndrome patients to increase stroke volume during exertion and their vulnerability to ventricular arrhythmias
- Treatment with cardiac glycosides, which could favor mechano-energetic uncoupling, should be discouraged in patients with Barth syndrome and left ventricular ejection fraction $>40\%$
- Instead, treatments with the potential to improve mechano-energetic coupling should be explored in future studies

Introduction

Barth syndrome (BTHS) is an X-linked multisystem disorder characterized by infantile onset of cardiomyopathy, skeletal myopathy, neutropenia, and growth retardation.¹ It is caused by mutations in the gene encoding tafazzin (*Taz*), a transacylase catalyzing maturation of cardiolipin (CL), a key phospholipid of the inner mitochondrial membrane (IMM).²⁻⁴ CL is required for structural organization of protein complexes in the IMM, in particular the electron transport chain (ETC) super-complexes (“respirasomes”).⁵ Defective CL maturation in BTHS destabilizes respirasomes⁶⁻⁹ and hampers production of adenosine triphosphate (ATP) by oxidative phosphorylation.^{7, 8, 10} Cellular models of BTHS revealed increased mitochondrial formation of reactive oxygen species (ROS),¹⁰⁻¹² and suppressing mitochondrial ROS prevented systolic dysfunction in a “heart-on-chip” inducible pluripotent stem cell (iPSC) model of BTHS,¹¹ suggesting a causal role of mitochondrial ROS in BTHS pathophysiology. Since ROS formation and elimination in cardiac mitochondria are intimately coupled to excitation-contraction (EC) coupling,¹³ we employed a mouse model with global *Taz*-knockdown (KD) to integrate mitochondrial function with ion handling in adult cardiac myocytes and hearts. Previous studies demonstrated that *Taz*-KD mice have decreased CL and a shift towards CL species with more saturated acyl groups, associated with ultrastructural and functional abnormalities of cardiac (and skeletal) muscle mitochondria.¹⁴⁻¹⁸ However, how these abnormalities cause cardiomyopathy is unresolved.

In cardiac myocytes, variations in energetic demand of EC coupling are matched by oxidative phosphorylation under the control of calcium (Ca^{2+}) and adenosine diphosphate (ADP),¹⁹ a process termed “mechano-energetic coupling”.²⁰ While ATP consumption at myofilaments and ion transporters oxidizes Krebs cycle-derived NADH and FADH_2 through

ADP-induced stimulation of respiration (“pull” condition), uptake of Ca^{2+} into mitochondria via the Ca^{2+} uniporter (MCU) stimulates Krebs cycle dehydrogenases to regenerate these pyridine nucleotides (“push”).²¹ In addition, the Krebs cycle regenerates NADPH for antioxidative capacity via NADP-linked isocitrate- and malate-dehydrogenases and the nicotinamide nucleotide transhydrogenase (NNT).^{13, 22, 23} Therefore, Ca^{2+} -driven metabolic adaptations sustain both ATP production and ROS elimination during cardiac workload transitions.^{19, 24}

We reported previously that alterations of EC coupling occurring in heart failure (HF) with reduced ejection fraction (HFrEF), such as decreased Ca^{2+} release from the sarcoplasmic reticulum (SR) and elevated cytosolic sodium (Na^+), hamper mitochondrial Ca^{2+} accumulation and thereby, provoke energy supply-and-demand mismatch and excessive ROS emission from mitochondria.²⁴⁻²⁶ Furthermore, elevated cardiac afterload drains mitochondrial NADPH via (reverse-mode) NNT towards NADH and ATP production, but at the cost of NADPH-coupled antioxidative capacity, triggering oxidative stress that causes cell death, cardiac remodeling, and dysfunction.²³ Consequently, targeting mitochondrial Ca^{2+} handling,²⁷ ROS^{28, 29} or CL^{23, 30-32} ameliorates HF progression in various animal models.

Despite this knowledge on mechano-energetic uncoupling in failing hearts, little information is available on these aspects in BTHS cardiomyopathy. BTHS often manifests with severe HF requiring heart transplantation in infancy, but then commonly transitions to a phenotype with milder systolic dysfunction, diastolic dysfunction and a lack of contractile reserve during physical exercise.³³⁻³⁷ Here, we show that cardiomyopathy in *Taz*-KD mice is in many aspects reminiscent of HF with *preserved* (HFpEF) rather than *reduced* ejection fraction, with increased myofilament Ca^{2+} affinity and slowed cross-bridge cycling velocity impairing myocardial relaxation and thereby, hindering diastolic filling of the left ventricle (LV). Furthermore,

disruption of mechano-energetic coupling rather than defects in respiratory chain^{6-8, 10} and/or increased formation of ROS¹⁰⁻¹² evolves as the primary mitochondrial defect in the *Taz*-KD mouse model of BTHS cardiomyopathy. As a central mechanism, severe downregulation of the MCU in cardiac mitochondria blunts adaptation of Krebs cycle activity to ATP consumption, thereby contributing to the limited contractile reserve during β -adrenergic stimulation. In addition, lack of Ca²⁺-induced Krebs cycle activation provides a trigger and a substrate for cardiac arrhythmias through mitochondrial oxidation and spontaneous activity in cardiac myocytes, and slowed intraventricular conduction *in vivo*. These data provide mechanistic insights into two major clinical problems in BTHS patients, i.e., the inability of the heart to increase LV ejection fraction (LVEF) during physical exercise³³ and the increased risk for arrhythmias.³⁸



Methods

The authors declare that all supporting data are available within the article and its online supplementary files. An expanded Methods section can be found in the Online data supplement. Animal procedures were approved by the local animal ethics committees (RUF-55.2.2-2532-2-804) and conducted in accordance with institutional guidelines. We used mice with short hairpin RNA-mediated KD of *Taz* as described previously¹⁴ that were obtained from Jackson Laboratories (B6.Cg-Gt(ROSA)26Sor^{tm37(H1/tet0-RNAi:Taz)Arte/ZkhuJ} (stock No. 014648). The genetic background of these mice is C57BL/129S6 and contains a functional NNT.

The generation of cardiac myocytes from iPSCs (WT-D2) of a control individual and a BTHS patient [TAZ10 (c.590 G>T)] was described previously.⁸ The study was approved by an

institutional review committee of Universitätsmedizin Göttingen⁸ and subjects gave informed consent.

Statistical analysis

Values are displayed as mean±SEM. Statistical parametric analyses were used after confirming that values followed a normal distribution. Statistical tests used for analysis are specified in each Figure legend and include two-way ANOVA followed by Bonferroni's multiple comparisons test, unpaired t tests, Fisher's exact test, and Chi-square test. If not specified otherwise, statistical analyses were performed using GraphPad Prism version 6.00 for Windows (GraphPad, <http://www.graphpad.com>). The n-numbers are indicated as numbers of cardiac myocytes / animals or as number of hearts or animals, depending on the Figure; the related information is provided in the Figure legend.



Results

Diastolic dysfunction and moderate systolic dysfunction in *Taz*-KD cardiomyopathy

Male and female mice with global shRNA-mediated KD of *Taz* (*Taz*-KD; **Figure I** in the Supplement) thrived normally up to an age of 20 weeks, but at 50 weeks, body weight was ~18% and heart weight (normalized to tibia length) ~11% lower compared to wild-type (WT) littermates (**Figure 1A-C, Table III** in the Supplement). Invasive assessment of LV hemodynamics *in vivo* at 10 weeks revealed unchanged heart rate, LV end-diastolic volume, ejection fraction and stroke volume, while maximal rates of contraction (dP/dt_{max}) and relaxation (dP/dt_{min}) were slowed by ~20% in *Taz*-KD hearts (**Figures 1D-G and IIA-C** in the Supplement). Also, load-independent parameters for systolic and diastolic function, i.e., end-systolic and end-diastolic pressure-volume relationships, and LV stroke work were modestly

impaired in *Taz*-KD vs. WT mice already at this age (**Figures 1H, I and IID** in the Supplement). Furthermore, the relaxation time-constant (τ) was prolonged and LV end-diastolic pressure modestly increased in *Taz*-KD vs. WT hearts, indicating diastolic dysfunction (**Figure IIE, F** in the Supplement). While female had slower rates of contraction and relaxation, and elevated EDPVR and LV end-diastolic pressures compared to male mice, no interaction existed between gender and genotype-related differences (**Figure III** in the Supplement).

Magnetic resonance imaging confirmed that at 10 weeks, LVEF, cardiac output, LV volumes and mRNA expression of atrial natriuretic peptide (*Anp*) were unchanged between *Taz*-KD and WT mice (**Figure 1J-M, Table IV** in the Supplement), while peak radial and circumferential systolic strain were reduced in *Taz*-KD (**Figure IV** in the Supplement). Between 10 and 15 weeks, cardiac output and LVEF modestly deteriorated in (male and female) *Taz*-KD mice, while LV cavity size remained unchanged at 20 and decreased at 50 weeks (**Figures 1J-L; V** in the Supplement, **Table IV** in the Supplement). Although LVEF remained >50% in *Taz*-KD mice up to 50 weeks, peak longitudinal, circumferential, and radial systolic strain further deteriorated (**Figure IV** in the Supplement) and *Anp* increased markedly after week 10 (**Figure 1M**), indicating progressive elevation of LV filling pressures. At 50 weeks, mitral inflow velocity assessed with Doppler echocardiography indicated that the E wave, reflecting early passive filling of the LV before atrial contraction, was lost in six of eight *Taz*-KD, but not WT mice (**Figure 1N**), further confirming impaired relaxation. Despite modestly increased gene expression of connective tissue growth factor (*Ctgf*, **Figure 1M**), no relevant increase in cardiac fibrosis occurred in *Taz*-KD mice even after 50 weeks (**Figure 1O, P**). Therefore, impaired relaxation is unlikely related to extracellular matrix remodeling, but rather to cardiac myocyte dysfunction.

Defects in excitation-contraction coupling in *Taz*-KD myocytes

To reveal the mechanisms underlying cardiac dysfunction, we analyzed sarcomere shortening and cytosolic Ca^{2+} concentrations ($[\text{Ca}^{2+}]_c$) in unloaded, field-stimulated cardiac myocytes from 10 week-old (w/o) mice. At baseline (0.5 Hz stimulation), *Taz*-KD myocytes displayed enhanced fractional sarcomere shortening compared to WT (**Figure 2A-C**), while the amplitude of $[\text{Ca}^{2+}]_c$ transients ($\Delta[\text{Ca}^{2+}]_c$) was unchanged (**Figure 2E, F**). Of note, the rate of $[\text{Ca}^{2+}]_c$ decay was faster in *Taz*-KD vs. WT myocytes (**Figure 2E, G**), while sarcomere re-lengthening kinetics were similar (**Figure 2D**). To induce a physiological increase in cardiac myocyte workload, we applied the β -adrenergic agonist isoproterenol (Iso; 30 nM) and increased stimulation frequency to 5 Hz. Fractional sarcomere shortening increased to similar values, while diastolic and systolic sarcomere lengths were shorter in *Taz*-KD vs. WT myocytes (**Figure 2A-C**). In contrast, the Iso/5 Hz-induced increase in diastolic and systolic $[\text{Ca}^{2+}]_c$ and thereby, also $\Delta[\text{Ca}^{2+}]_c$ were blunted in *Taz*-KD myocytes, while rates of $[\text{Ca}^{2+}]_c$ decay accelerated to similar maximal levels in both groups (**Figure 2E-G**).

In murine cardiac myocytes, ~90% of cytosolic Ca^{2+} is removed by the SR Ca^{2+} ATPase (SERCA) during steady-state $[\text{Ca}^{2+}]_c$ transients, while ~10% is removed by the $\text{Na}^+/\text{Ca}^{2+}$ -exchanger (NCX).³⁹⁻⁴¹ To determine the contribution of SERCA and NCX towards $[\text{Ca}^{2+}]_c$ removal and assess SR Ca^{2+} load, we applied caffeine to rapidly open ryanodine receptors, releasing SR Ca^{2+} after pacing at 0.5 Hz and Iso/5 Hz, respectively. While caffeine-induced SR Ca^{2+} release and fractional SR Ca^{2+} release during steady-state $[\text{Ca}^{2+}]_c$ transients were similar between genotypes under either condition (**Figure 2I-K**), Iso/5 Hz-induced accumulation of diastolic $[\text{Ca}^{2+}]_c$ and net cellular Ca^{2+} load (i.e., maximal $[\text{Ca}^{2+}]_c$ after caffeine-induced SR Ca^{2+} release) were lower in *Taz*-KD vs. WT myocytes (**Figure 2L-N**). Again, rates of $[\text{Ca}^{2+}]_c$ decline

during steady-state $[Ca^{2+}]_c$ transients (reflecting mostly SERCA activity; **Figure VI** in the Supplement) were faster in *Taz*-KD vs. WT myocytes at baseline, but increased to similar maximal rates in both genotypes at Iso/5 Hz (**Figure 2G, O**). Furthermore, also $[Ca^{2+}]_c$ decay kinetics after caffeine, reflecting mostly NCX activity,³⁹ were accelerated in *Taz*-KD vs. WT myocytes at 0.5 Hz (in trend) and Iso/5 Hz ($p<0.05$), respectively (**Figure 2P**), but yet these rates were an order of magnitude slower (τ ~10-fold longer) than SERCA rates (**Figure 2O**). These data indicate that $[Ca^{2+}]_c$ decay is hastened by accelerated SERCA and NCX activities at baseline, with a blunted SERCA reserve being recruited during β -adrenergic stimulation in *Taz*-KD vs. WT myocytes.

Western-blot analyses in 10 w/o hearts revealed unchanged protein expression of SERCA, while its inhibitory protein phospholamban (PLN) was ~50% downregulated in *Taz*-KD vs. WT hearts (**Figure VIIA-C** in the Supplement). Furthermore, phosphorylation of PLN at protein kinase A (PKA) and Ca^{2+} /calmodulin-dependent protein kinase II (CaMKII)-specific sites (serine-16 and threonine-17, respectively), by which the inhibition of SERCA by PLN is relieved,^{39, 40} was increased in relation to total PLN protein (**Figure VIIB, D** in the Supplement). In cardiac myocytes from aged (50 w/o) *Taz*-KD mice, a similar phenotype evolved as in young (10 w/o) mice, with shorter sarcomere length and enhanced fractional shortening at Iso/5 Hz despite a blunted increase of $\Delta[Ca^{2+}]_c$ (**Figure VIIIA-D** in the Supplement). In agreement with progressive diastolic dysfunction *in vivo* (**Figure 1G, I**), sarcomere re-lengthening substantially slowed in 50 w/o *Taz*-KD vs. WT myocytes at baseline and Iso/5 Hz (**Figure 2D**). When plotting sarcomere length against $[Ca^{2+}]_c$, sarcomeres were shorter at any given $[Ca^{2+}]_c$ at 10 (**Figure 2H**) or 50 weeks (**Figure VIIIE, F** in the Supplement), pinpointing increased Ca^{2+} affinity of myofilaments to underlie diastolic dysfunction in *Taz*-KD myocytes.

To resolve this, we assessed force- Ca^{2+} relationships in membrane-permeabilized and mechanically preloaded myocytes from young (10 w/o) mice. While cross-sectional area, maximal and passive force generation, and Ca^{2+} -cooperative activation remained unchanged between genotypes (**Table V** in the Supplement), *Taz*-KD myocytes displayed a leftward shift in the force/pCa relationship (**Figure 2Q**), confirming elevated myofilament Ca^{2+} sensitivity (EC_{50} 2.2 ± 0.1 vs. 3.0 ± 0.2 μM [Ca^{2+}] for *Taz*-KD vs. WT; $p=0.0002$). Of note, rate constants of tension redevelopment after re-stretching (k_{TR}) plotted against corresponding isometric forces, indexing cross-bridge cycling velocity,^{42, 43} were (s)lower in *Taz*-KD than WT myocytes (**Figure 2R**). In summary, increased myofilament Ca^{2+} sensitivity and decreased cross-bridge cycling velocity are early defects of EC coupling in *Taz*-KD hearts, which are partly compensated by accelerated SERCA- and NCX-dependent [Ca^{2+}]_c decay kinetics at young age. This preactivation of Ca^{2+} handling, however, blunts the recruitable SERCA reserve during β -adrenergic stimulation already at 10 weeks of age. With aging, diastolic dysfunction *in vivo* (**Figure 1I**) and *in vitro* (**Figure 2D**) surfaces already in the absence of β -adrenergic stimulation, despite maintained preactivated SERCA activity (**Figure VIID** in the Supplement). Since cross-bridge cycling and SERCA activity are major cellular ATP consumers,³⁹ these alterations pose an extra energetic burden on mitochondria in *Taz*-KD myocytes.

Mild respiratory dysfunction, but unchanged ROS emission in cardiac *Taz*-KD mitochondria

Since *Taz*-knockdown impairs synthesis of mitochondrial CL, which is required for the stability of the ETC supercomplexes, we analyzed structural organization and function of the ETC in cardiac mitochondria. Blue native gel electrophoresis (BN-PAGE) revealed destabilization of supercomplexes (I-III_n-IV_n) and increased abundance of monomeric cytochrome *c* oxidase in 10

w/o *Taz*-KD mitochondria, which was, however, not further aggravated after 50 weeks (**Figure 3A**). In line with previous studies,^{7, 8, 44} using pyruvate/malate as substrates, submaximal and maximal ADP-coupled (“state 3”) respiration was lower in cardiac mitochondria from 10 w/o *Taz*-KD vs. WT mice (**Figure 3B**). However, at 20 and 50 weeks of age, respiratory capacity deteriorated in WT animals, and was no longer different in *Taz*-KD vs. WT mice (**Figures 3E; IXA, B** in the Supplement). Interestingly, neither mitochondrial $\cdot\text{O}_2^-$ formation nor H_2O_2 emission were different in the absence or presence of ADP at any age (**Figures 3C, D, F, G; IXC-E** in the Supplement).

Loss of the MCU abrogates Ca^{2+} uptake in cardiac mitochondria of *Taz*-KD mice

Since mitochondrial Ca^{2+} uptake regulates mitochondrial ATP production and antioxidative capacity in cardiac myocytes,¹⁹ we determined Ca^{2+} retention capacity of isolated cardiac mitochondria from 10 w/o animals by applying sequential Ca^{2+} pulses (10 μM) to isolated mitochondria, monitoring extramitochondrial $[\text{Ca}^{2+}]$. In WT mitochondria, each elevation of extramitochondrial Ca^{2+} was followed by an exponential decay, indicating Ca^{2+} uptake into mitochondria (**Figure 4A**). After several pulses, the rate of Ca^{2+} uptake slowed and eventually, Ca^{2+} was released from mitochondria, which was prevented by cyclosporine A, an inhibitor of the permeability transition pore (PTP). Strikingly, Ca^{2+} uptake was absent in *Taz*-KD mitochondria, unaffected by cyclosporine A (**Figure 4A**), ruling out premature PTP opening. The same occurred in mitochondria from 20 w/o mice (**Figure IXF** in the Supplement). As an underlying mechanism, BN-PAGE analysis in cardiac mitochondria of *Taz*-KD and global *Mcu*-knockout (KO) mice⁴⁵ revealed that all three MCUa-specific bands decreased in 10 w/o *Taz*-KD mitochondria, reflecting loss of the pore-forming MCUa subunit from the uniporter complex (**Figure 4B**). Western blot analyses confirmed reduced protein, but not mRNA levels of

MCUa in *Taz*-KD hearts at any age (**Figure 4C, D; IXG, H** in the Supplement). This was confirmed in iPSC-derived cardiac myocytes obtained from one BTHS patient compared to a healthy control (**Figure 4E**). In contrast, expression of MCUb, which inhibits MCU-dependent Ca^{2+} uptake,^{46, 47} increased (**Figures 4C; IXG, H** in the Supplement). While protein levels of MCU component MCUR1 were increased, expression of other MCU complex members, i.e., MICU1, MICU2 and EMRE, were unchanged in 10 w/o *Taz*-KD mice (**Figure 4C**).

Mitochondrial Ca^{2+} uptake is preserved in skeletal muscle and brain of *Taz*-KD mice

Besides cardiomyopathy, BTHS patients develop skeletal myopathy with exercise intolerance and fatigue.⁴⁸ In skeletal muscle mitochondria, ETC structure and H_2O_2 emission were unaffected at 10 and 20 weeks, while at 50 weeks, ADP-stimulated respiration was reduced in *Taz*-KD vs. WT (**Figure XA-F** in the Supplement). In contrast to cardiac-, skeletal muscle mitochondria displayed normal Ca^{2+} uptake at all ages (**Figure XIA-C** in the Supplement) despite modest structural remodeling of the MCU complex and a trend towards lower protein abundance of MCUa, with other MCU complex subunits unchanged (**Figure XID, E** in the Supplement). In *Taz*-KD brain mitochondria, Ca^{2+} uptake, MCUa protein levels and MCU complex structure were preserved (**Figure XIF-H** in the Supplement). These data indicate that loss of MCUa protein primarily affects Ca^{2+} uptake in cardiac mitochondria, whereas in skeletal muscle mitochondria, Ca^{2+} accumulation is preserved despite modest changes in MCUa levels and MCU complex structure. These differences might be explained by tissue-specific CL composition of the IMM and by the higher MCU current density in murine skeletal muscle compared with cardiac mitochondria.^{49, 50}

Defective mitochondrial Ca^{2+} uptake provokes pyridine nucleotide oxidation during workload transitions in *Taz*-KD cardiac myocytes

To assess the consequences of MCU deficiency in mitochondria integrated into their physiological environment in intact cardiac myocytes, we monitored $[Ca^{2+}]_c$ and mitochondrial Ca^{2+} concentrations ($[Ca^{2+}]_m$) in the same cells, employing a patch-clamp based technique.²⁵ In fact, despite unchanged $\Delta[Ca^{2+}]_c$, the amplitude of $[Ca^{2+}]_m$ transients was diminished in *Taz*-KD vs. WT myocytes and failed to further increase in response to Iso/5 Hz, blunting mitochondrial Ca^{2+} accumulation (**Figure 5A-C**).

During workload transitions, ADP accelerates electron flux along the ETC, thereby oxidizing NADH and FADH₂.¹⁹ Under physiological conditions, $[Ca^{2+}]_m$ accumulation stimulates Krebs cycle dehydrogenases to maintain adequate supply of reducing equivalents to the ETC.^{19, 51} In WT myocytes, NAD(P)H and FAD redox states were largely maintained during workload transitions (**Figure 5D, E**). In contrast, these abruptly oxidized without any Ca^{2+} -mediated recovery during Iso/5 Hz in *Taz*-KD myocytes, whereas mitochondrial membrane potential ($\Delta\Psi_m$) was maintained (**Figure 5D-F**). While baseline NAD(P)H/FAD redox states were similar in myocytes of 10 w/o mice (**Figure 5D, E**), these were more oxidized in 20 and 50 w/o *Taz*-KD vs. WT myocytes, which further aggravated during 5 Hz stimulation (**Figure XII** in the Supplement). Of note, at 20 and 50, but not 10 weeks, *Taz*-KD myocytes displayed more spontaneous (i.e., non-stimulated) contractions compared to WT after stepping back to 0.5 Hz (**Figure 5G, H**).

To interrogate whether NAD(P)H/FAD oxidation and arrhythmias are related to defective mitochondrial Ca^{2+} uptake, Ca^{2+} extrusion via the mitochondrial Na^+/Ca^{2+} exchanger (NCLX) was inhibited with CGP-37157.²⁵ In fact, NCLX-inhibition reduced NAD(P)H and FAD redox states before and during Iso/5 Hz (**Figure 5I**) and decreased the number of non-stimulated beats in *Taz*-KD myocytes (**Figure 5J**).

Mitochondrial ROS emission is prevented by upregulation of ROS-detoxifying capacity in *Taz*-KD cardiac myocytes

Since in our previous studies, inhibiting mitochondrial Ca^{2+} accumulation oxidized NAD(P)H and increased mitochondrial ROS emission,^{25, 26} we expected that also in *Taz*-KD myocytes, NAD(P)H oxidation would elevate mitochondrial ROS. However, oxidation of the non-selective ROS indicator DCF was similar in myocytes from 10 w/o *Taz*-KD vs. WT mice at 0.5 Hz and Iso/5 Hz stimulation, respectively (**Figure 6A**). When myocytes were exposed to 1 mM extracellular H_2O_2 , however, the increase in DCF fluorescence was ~50% lower in *Taz*-KD versus WT myocytes (**Figure 6B, C**), indicating augmented cellular H_2O_2 -eliminating capacity. This was consistent with 2-fold increased protein expression of H_2O_2 -eliminating catalase and glutathione peroxidase 1 (GPX1) at 10 weeks, while expression of $\cdot\text{O}_2^-$ eliminating superoxide dismutases (SOD) 1 and 2 as well as peroxiredoxin (PRDX) isoforms 1-3 were unchanged (**Figure 6D**). At 20 and 50 weeks, however, catalase and GPX1 upregulation ceased, and at 50 weeks, expression of mitochondrial PRDX3 and SOD2 were reduced in *Taz*-KD vs. WT myocytes (**Figure 6D**).

To monitor H_2O_2 directly *in vivo*, we crossed WT and *Taz*-KD mice with mice expressing an H_2O_2 -specific fluorescence reporter in the mitochondrial matrix (mito-roGFP2-Orp1).⁵² The redox state of mito-roGFP2-Orp1 (reporting H_2O_2) was similar in WT and *Taz*-KD hearts at 20 weeks (**Figure 6E, F**) and was rather reduced in *Taz*-KD vs. WT hearts at 50 weeks (**Figure 6E**). Also, nuclear staining of 8-hydroxy-2'-guanosine as a marker of intracellular oxidative stress was not significantly different between genotypes (**Figure 6G**). Aconitase activity as an indirect, yet unspecific index of mitochondrial ROS formation was decreased in 50 w/o *Taz*-KD vs. WT hearts (**Figure 6H**).

These results suggest that while ROS formation at the respiratory chain is unaltered, the anticipated increase of H₂O₂ emission from mitochondria due to insufficient Ca²⁺-stimulated and Krebs cycle-mediated NADPH regeneration in *Taz*-KD myocytes may be counterbalanced by compensatory upregulation of H₂O₂-detoxifying enzymes at young age. Although this upregulation vanishes at older age, no clear increase in ROS occurs despite NAD(P)H oxidation in *Taz*-KD cardiac myocytes.

Energetic deficit underlies compromised systolic reserve in Taz-KD myocytes

A so far unresolved issue is that while *Taz*-KD mice had mildly impaired systolic function *in vivo* (**Figures 1 and ID-I** in the Supplement), isolated cardiac myocytes displayed preserved or even supranormal sarcomere shortening (**Figure 2A-C**), likely related to increased myofilament Ca²⁺ affinity (**Figure 2Q**). However, in *unloaded* myocytes, energetic demand is underestimated compared to the *in vivo* situation since mechanical *preload* of cardiac myocytes (or muscle) increases O₂ and ATP consumption.²⁰ Sarcolemmal ATP-dependent K⁺ channels (K_{ATP}) sense the intracellular ATP/ADP ratio: when ATP levels drop, K_{ATP} channels conduct K⁺ efflux that hyperpolarizes the cell membrane.^{20, 53} This shortens the action potential and reduces Ca²⁺ influx via L-type Ca²⁺ channels, preventing cytosolic Ca²⁺ overload during metabolic stress.^{20, 53} In normoxic cardiac myocytes, K_{ATP} channels are closed,²⁰ but sensitized to diminished mitochondrial ATP production by pinacidil.^{54, 55}

We exposed myocytes to workload transitions as in **Figure 2** in the absence or presence of pinacidil or the K_{ATP} channel blocker HMR-1098.⁵⁶ While in WT myocytes, neither of these affected basal or maximal sarcomere shortening, pinacidil blunted the increase in sarcomere shortening in response to Iso/5 Hz in *Taz*-KD myocytes (**Figure 7A**), suggesting that drug-

primed K_{ATP} channels are activated by a reduced cellular ATP/ADP ratio under these conditions, decreasing Ca^{2+} influx.

We next employed a technology developed by Prosser *et al.*⁵⁷ and Helmes *et al.*,⁵⁸ by which isolated cardiac myocytes are pre-stretched with glass fibers to exert isometric contractions (**Figure 7B**). Preload-dependent potentiation of force by the Frank-Starling mechanism is matched by an increase in O_2 (and therefore ATP) consumption.²⁰ Accelerating stimulation rate from 1 to 4 Hz in pre-stretched myocytes further increased systolic force generation in WT myocytes, caused by intracellular Ca^{2+} accumulation and SR Ca^{2+} loading^{39, 59} (“Bowditch Treppe”; **Figure 7B-E**). When stepping back from 4 to 1 Hz, the transient (“post-rest”-like) potentiation of force is explained by increased SR Ca^{2+} loading during the prior 4 Hz stimulation.^{39, 59} Strikingly, both the Bowditch Treppe and post-rest-like potentiation of force were completely blunted in *Taz*-KD myocytes (**Figure 7C-E**). Furthermore, while in *unloaded* myocytes, systolic sarcomere shortening was preserved at Iso/5 Hz (**Figure 2C**), force generation was substantially decreased in mechanically *preloaded* *Taz*-KD myocytes at 4 Hz (**Figure 7C-E**). Therefore, mechanical preload, which elevates cellular ATP consumption,²⁰ deteriorates systolic force generation in *Taz*-KD myocytes, while in the presence of saturating ATP and phosphocreatine in permeabilized myocytes, maximal force generation was maintained (**Figure 2Q, Table V** in the Supplement). Together, these data suggest that metabolic adaptation during elevated workload rather than ATP-producing capacity of mitochondria *per se* contributes to systolic dysfunction in *Taz*-KD mice.

Impaired inotropic reserve and prolonged QRS duration in Taz-KD mice in vivo

To test the relevance of these observations *in vivo*, we assessed LV function by pressure-volume analyses in 10 w/o mice. As reported above (**Figures 1D-I**), LVEF, stroke volume and cardiac

output were unchanged, but dP/dt_{\max} modestly reduced in *Taz*-KD vs. WT mice under resting conditions. In response to intravenous infusion of the β_1 -adrenergic agonist dobutamine, heart rate increased similarly in both genotypes (**Figure 7F**). In contrast, the inotropic response, indexed by changes in dP/dt_{\max} , LV stroke volume, and LVEF, was completely blunted in *Taz*-KD compared to WT mice (**Figures 7G-H**). MCUa downregulation in *Taz*-KD hearts correlated with suppression of the inotropic response to β_1 -adrenergic stimulation (**Figures 7I; XIII** in the Supplement), comparable to findings in *Mcu*-KO mice.⁶⁰ However, pretreatment of *Taz*-KD animals with the NCLX-inhibitor CGP-37157 could not recover the inotropic response (**Figures 7G-I; XIII** in the Supplement).

We reasoned that NCLX inhibition did not improve the inotropic response because β -adrenergic stimulation is additionally dampened by preactivation of SERCA (**Figure 2; VII** in the Supplement). Therefore, we sought to monitor another marker of intracellular ATP and at the same time, gain additional insight on whether the mitochondrial Ca^{2+} defect may predispose to arrhythmias. We recorded ECG in *Taz*-KD and WT mice and observed that QRS duration is prolonged by ~30% in *Taz*-KD versus WT animals, and remained prolonged during modest β_1 -adrenergic stimulation with dobutamine (**Figure 7J, K**). Because propagation of the electrical signal between cardiac myocytes is governed by connexin 43, which relies on ATP-dependent phosphorylation and is inactivated by focal energy depletion,⁶¹ we reasoned that intracellular ATP shortage secondary to impaired mitochondrial Ca^{2+} uptake might account for QRS prolongation in *Taz*-KD mice. Accordingly, NCLX inhibition with CGP-37157 shortened QRS duration in *Taz*-KD, but not WT mice, resolving the differences between genotypes (**Figure 7K**). These data indicate that impaired mitochondrial Ca^{2+} uptake slows intraventricular conduction in

Taz-KD hearts, possibly related to energetic depletion,⁶¹ and that boosting mitochondrial Ca^{2+} accumulation can resolve this defect during β -adrenergic stimulation.

Discussion

BTHS can manifest with a severe form of cardiomyopathy, potentially lethal or requiring heart transplantation in infancy. The clinical phenotype of BTHS cardiomyopathy is both heterogeneous and dynamic, and its pathophysiology largely unresolved. The most commonly reported manifestation is dilated cardiomyopathy (DCM), but often in combination with morphological aspects of hypertrophic (HCM) and/or non-compaction cardiomyopathy.^{34-37, 62}

While in the first weeks of life, a phenotype of DCM with systolic dysfunction is more common, LV dilation regresses and systolic function recovers during the first year(s) of life in the majority of patients.^{34, 35} In fact, most patients eventually enter a phase in which LVEF is preserved (at ~50%) and remains stable³⁶ or only mildly deteriorates over the following two decades.³⁷

However, although LVEF is preserved at rest, diastolic function is compromised and LVEF does not increase during exercise,³³ resembling the clinical phenotype of HFpEF⁶³⁻⁶⁵ and likely contributing to exercise intolerance of BTHS patients.³³ Finally, patients with BTHS can suffer or die from ventricular arrhythmias.^{38, 66}

Here, we show that cardiomyopathy of *Taz*-KD mice is characterized by early diastolic and modest systolic dysfunction, and more closely resembles HFpEF than HFrEF, recapitulating the phenotype of those BTHS patients who do not develop (or recovered from) severe pump failure during infancy.^{34-37, 62} Progressive diastolic dysfunction *in vivo* in the absence of relevant fibrosis is explained by elevated myofilament Ca^{2+} affinity and slowed cross-bridge cycling, a feature

characteristic of hereditary forms of HCM, but not DCM.⁶⁷ To compensate for sarcomeric relaxation deficits, cytosolic Ca²⁺ decay is accelerated in *Taz*-KD myocytes through increased SERCA and NCX activities under “resting” conditions, which largely exploits the inotropic and lusitropic reserve during β -adrenergic stimulation *in vivo* (**Figure 8**). This contrasts with the defects in EC coupling in myocytes from animal models⁶⁸ or patients⁶⁹ with HFrEF, where *reduced* SERCA activity and SR Ca²⁺ load cause systolic and diastolic dysfunction. Furthermore, our data contrast with a study on the same *Taz*-KD mouse model in which reduced SERCA activity (probed by biochemical assays) was suggested to explain diastolic and systolic dysfunction in BTHS cardiomyopathy.⁷⁰ Here, we can trace SERCA activation to downregulation of its inhibitory regulator PLN, as well as PLN hyperphosphorylation by PKA and CaMKII. The latter is in agreement with increased CaMKII activity in a different BTHS mouse model, in which cardiac myocyte-specific *Taz*-knockout induced a DCM-like phenotype with systolic dysfunction⁷¹ and ventricular arrhythmias that were attributed to ROS-induced CaMKII activation.⁷²

As the primary mitochondrial defect, we identified selective deficiency of MCU protein, but not mRNA, which destabilized the MCU complex and abrogated Ca²⁺ uptake into mitochondria from *Taz*-KD hearts (**Figure 8**). This agrees with a recent report that revealed that CL is required for MCU complex stability in yeast mitochondria and confirmed this in myocardium from patients with BTHS.⁷³ However, this study was mostly based on a minimal MCUa-EMRE complex recombinantly expressed in the baker's yeast *Saccharomyces cerevisiae* that does not contain an intrinsic MCU-like channel. Furthermore, the physiological implications and disease relevance of these results were not experimentally addressed. Our comprehensive analyses extend these observations by showing that the MCU defect is specific for *Taz*-deficiency in

heart, but not skeletal muscle or brain mitochondria. In contrast, respiratory chain function deteriorates with age in skeletal muscle-, but not cardiac mitochondria of *Taz*-KD mice, suggesting important tissue-specific differences of CL deficiency causing cardiac- or skeletal muscle myopathy in BTHS, respectively. Another possible explanation for these tissue-specific alterations is a difference in skeletal muscle fiber composition; we cannot exclude that *Taz*-KD mice develop a compensatory increase in fast-twitch muscle fibers, which are predominantly glycolytic and have a lower total CL pool.^{74, 75}

During physiological workload transitions, lack of mitochondrial Ca^{2+} uptake prevents Krebs cycle activation and regeneration of reduced pyridine nucleotides in *Taz*-KD cardiac myocytes (**Figure 8**). Our results are supported by computational modeling data, predicting that removal of Ca^{2+} -dependent Krebs cycle activation oxidizes NADH after increasing pacing frequency.⁷⁶ Furthermore, they are in line with results of our previous studies in guinea pig cardiac myocytes with pharmacological inhibition of the MCU²⁶ or acceleration of NCLX-dependent mitochondrial Ca^{2+} extrusion (at elevated $[\text{Na}^+]_i$),²⁵ but also studies on mice with genetic deletion of the MCU.⁶⁰ Based on our previous results, we anticipated increased emission of H_2O_2 from mitochondria due to depletion of antioxidative NADPH.^{23, 26} However, this was prevented by upregulation of H_2O_2 -eliminating catalase and GPX1, but not of $\cdot\text{O}_2^-$ -eliminating SOD1 or SOD2 in *Taz*-KD hearts. We also ruled out increased $\cdot\text{O}_2^-$ formation at the respiratory chain or H_2O_2 emission from isolated cardiac and skeletal muscle mitochondria, further supported by lack of mitochondrial H_2O_2 elevation in hearts *in vivo* as detected with the sensitive and specific H_2O_2 sensor mito-roGFP2-Orp1.⁵²

These data are in contrast to previous reports of increased ROS formation in BTHS cell models,¹⁰⁻¹² one of which assigned ROS a causal role for systolic dysfunction in an iPSC model

of BTHS.¹¹ Furthermore, our data to some extent contrast with another study⁴⁴ reporting increased H₂O₂ emission from cardiac, but not skeletal muscle mitochondria respiring on succinate in the absence of rotenone, a condition which favors $\bullet\text{O}_2^-$ formation at complex I via reverse electron transfer.⁷⁷ In the mentioned study,⁴⁴ *Taz* was knocked down in C57BL/6J mice, in which a loss-of-function mutation of the mitochondrial transhydrogenase favors H₂O₂ emission in working cardiac myocytes.²³ Conversely, our data agree with a recent study that observed no increase in ROS formation at eleven different sites within cardiac and skeletal muscle mitochondria of *Taz*-KD mice on a C57BL/6NJ background,⁷⁸ which (in contrast to C57BL/6J) *does* contain a functional transhydrogenase,²³ as does our model. Taken together, our data generated by a broad spectrum of methods *in vitro* and *in vivo* argue against a relevant role of mitochondrial ROS in the pathophysiology of cardioskeletal myopathy in the *Taz*-KD model of BTHS.

Our results may explain why (further) overexpression of catalase does not alter the cardiac phenotype in *Taz*-KD mice.⁴⁴ Furthermore, we observed previously that *Taz*-deficiency dampens ROS production during hypoxia, which hampered HIF-1 α signaling *in vitro* and was associated with aggravated cardiac hypertrophy and failure in response to pressure overload *in vivo*,¹² assigning mitochondrial ROS a potential protective role as framed in the concept of “mitohormesis”.⁷⁹ Although we did not detect upregulation of nuclear factor erythroid 2-related factor (Nrf2; data not shown), a key transcription factor in ROS-dependent mitohormesis,⁸⁰ in 10 week-old *Taz*-KD hearts, one cannot exclude that redox-dependent processes triggered mitohormesis earlier in development of *Taz*-KD hearts, such as the observed upregulation of catalase and glutathione peroxidase. Altogether, these findings discourage previously suggested strategies to treat BTHS patients with antioxidants.^{11, 81, 82}

One caveat is that our *Taz*-KD mice retain ~10% of *Taz* mRNA, which might explain some of the differences to cell systems¹⁰⁻¹² or mice^{71, 72} with complete knock-out of *Taz*. Potentially, such residual *Taz*-expression may account for the milder cardiac phenotype of *Taz*-KD compared to *Taz*-knockout mice,^{71, 72} in which mitochondrial ROS and oxidative stress might become relevant to the progression of cardiomyopathy; in fact, the differences between the *Taz*-KD and -knockout model potentially reflect the heterogeneity of BTHS cardiomyopathy in humans. In contrast, age as a confounder can be largely excluded to explain differences between our and previous studies, since mitochondrial ROS were not elevated at any age in our *Taz*-KD mice.

Patients with BTHS are at risk for sudden cardiac death,³⁸ but the mechanisms underlying ventricular arrhythmias are unknown. Arrhythmias typically require a trigger and a substrate. As a trigger, we observed cellular arrhythmias in *Taz*-KD myocytes after isoproterenol-induced oxidation of the mitochondrial NAD(P)H redox state, and both NAD(P)H oxidation and cellular arrhythmias were blunted by the NCLX-inhibitor CGP-37157. Furthermore, as a potential substrate, we observed slowed intraventricular conduction in *Taz*-KD hearts *in vivo*, which was completely reversed by NCLX-inhibition. These data indicate that the defect in mitochondrial Ca²⁺ uptake provides a trigger and a substrate for arrhythmias.

In this context, the cardiac phenotype of *Taz*-KD mice has many similarities with mouse models of HCM, in which increased myofilament Ca²⁺ affinity (induced by troponin T mutation I79N) underlies afterdepolarizations in isolated cardiac myocytes *in vitro*,⁸³ but also QRS broadening and ventricular arrhythmias *in vivo*.⁶¹ The latter could be traced to focal energy depletion in cardiac myocytes, since increased myofilament Ca²⁺ affinity “drains” ATP, dephosphorylates connexin-43 and slows intraventricular conduction during β -adrenergic stimulation as an established substrate for re-entry arrhythmias.⁶¹ In a parallel (yet unpublished)

study, we observed that in these same troponin T I79N mutant mice, NAD(P)H oxidation and arrhythmias in isolated cardiac myocytes and whole hearts were blunted by CGP-37157, indicating that a mismatch of ADP-induced oxidation and Ca^{2+} -induced regeneration of NAD(P)H accounts for the vulnerability for arrhythmias in HCM. Therefore, in *Taz*-KD mice, increased myofilament Ca^{2+} affinity and defective mitochondrial Ca^{2+} uptake conspire to oxidize mitochondrial NADH and NADPH, where NADH oxidation may limit ATP regeneration, and NADPH depletion may cause oxidation of cellular ion transport systems, such as ryanodine receptors (RyR2), to account for cellular arrhythmias. Along similar lines, Liu et al.⁷² reported redox activation of CaMKII with subsequent phosphorylation of RyR2 in *Taz*-knockout mice, which likely aggravate this process.

It is a long-held concept that mitochondrial Ca^{2+} uptake matches metabolic output to cardiac workload by Ca^{2+} -induced activation of Krebs cycle dehydrogenases (**Figure 8**).^{19, 51, 84, 85} However, direct experimental evidence for this concept is challenging. We approached this problem in several ways. First, by sensitizing sarcolemmal K_{ATP} channels to variations in mitochondrial ATP production with pinacidil, systolic sarcomere shortening was compromised in *Taz*-KD, but not WT myocytes, likely mediated by K_{ATP} channel-induced hyperpolarization of the cell membrane that limits cellular Ca^{2+} influx.^{20, 53} Second, by comparing maximal sarcomere shortening in *unloaded* cardiac myocytes with force generation in mechanically *preloaded* cardiac myocytes, where only in preloaded myocytes, systolic dysfunction unfolds in *Taz*-KD vs. WT myocytes, although in mechanically preloaded, but permeabilized cardiac myocytes in the presence of sufficient (external) ATP, maximal force generation was similar between both genotypes. Third, by monitoring QRS duration *in vivo*, which relies on connexin 43 phosphorylation by intracellular ATP,⁶¹ increasing mitochondrial Ca^{2+} accumulation by NCLX

inhibition dissolved the differences in intraventricular conduction between both genotypes, suggesting that mitochondrial Ca^{2+} deficiency contributes to intracellular ATP shortage. In contrast, NCLX inhibition was unable to restore the inotropic response to β -adrenergic stimulation, which is likely additionally limited by SERCA preactivation.

Together, these data suggest that defective Ca^{2+} -dependent energy supply-and-demand-matching limits ATP regeneration required for maximal force production, but also intraventricular electrical conduction. Additional support for this concept comes from studies in *Mcu*-KO animals, in which delayed metabolic adaptation abrogates the acute increase in contractile performance induced by isoproterenol infusion *in vivo*.⁶⁰ Mitochondrial Ca^{2+} -driven metabolic adaptations, and thereby the bioenergetic mismatch resulting from MCU deficiency, might be even more relevant in humans than rodents, since the increase of cardiac output (and therefore, also ATP consumption) during exertion is ~0.5-fold in mice,⁸⁶ but ~4-fold in humans,⁸⁷ likely requiring a higher degree of Ca^{2+} -induced adaptation of Krebs cycle activity.

Conclusions

Our data identify disruption of the mechano-energetic coupling reserve (**Figure 8**) rather than – as previously suggested – decreased respiration or oxidative stress as a primary defect in the *Taz*-KD model of BTHS cardiomyopathy, which is characterized by diastolic more than systolic dysfunction *in vitro* and *in vivo*. These data help explain two major clinical problems in BTHS patients, i.e., the inability of the heart to increase LVEF during physical exercise,³³ which is specific for BTHS, but not other forms of mitochondrial cardiomyopathies,⁸⁸ and to some extent, the increased risk for arrhythmias.³⁸

This has implications for the treatment of patients with BTHS, in whom the use of cardiac glycosides is still common,³⁴ although these cause mechano-energetic uncoupling and ventricular tachycardia through hampering mitochondrial Ca^{2+} uptake.⁸⁹ In fact, in a case series of five patients with BTHS who suffered from ventricular tachycardia or fibrillation, two of whom died suddenly while playing, all five had digoxin as the only common medication, although only one of these patients had a typical DCM-like phenotype with relevant systolic dysfunction, while the remaining four had largely preserved EF,³⁸ comparable to the *Taz*-KD mouse model of the current study. Therefore, based on the results of our study, we suggest that the use of digoxin in BTHS should be discouraged,³⁴ especially in those patients with an LVEF >40%, while future efforts should be directed at probing treatments that improve mechano-energetic coupling through lowering energetic demand (i.e., by myosin modulators⁹⁰) and/or improve mitochondrial Ca^{2+} uptake (i.e., by SGLT2-inhibitors⁹¹).

Acknowledgements

We thank Michelle Gulentz, Nina Schnellbach, and Annette Berbner for technical assistance.

Sources of Funding

The project was initiated by support from the German Heart Foundation (Margret Elisabeth Strauß-Projektförderung to CM). CM is/was supported by the Barth Syndrome Foundation, the German Research Foundation (DFG; Ma 2528/7-1, SFB 894, TRR-219) and the German Federal Agency for Education and Research (BMBF; 01EO1504). JD is supported by the DFG (DU1839/2-1), the BMBF and the Barth Syndrome Foundation. MH is supported by the DFG (SFB 894 and SFB 1027). MvdL is supported by the Barth Syndrome Foundation and the DFG

(SFB 894). PR is funded by the European Research Council (ERC) Advanced Grant (ERCAdG No. 339580), DFG (SFB1002, project A06), and the DFG under Germany's Excellence Strategy - EXC 2067/1- 390729940. KS is supported by the DFG (SCHU1600/6-1).

Disclosures

CM, UL and MB received speaker and consultancy honoraria from Boehringer Ingelheim and AstraZeneca.

Supplemental Materials

Expanded Methods

Online-only **Figures I-XIII.**

Online-only **Tables I-V.**

References ⁹²⁻⁹⁹.



Circulation

References

1. Barth PG, Scholte HR, Berden JA, Van der Klei-Van Moorsel JM, Luyt-Houwen IE, Van 't Veer-Korthof ET, Van der Harten JJ, Sobotka-Plojhar MA. An X-linked mitochondrial disease affecting cardiac muscle, skeletal muscle and neutrophil leucocytes. *J Neurol Sci.* 1983;62:327-55.
2. Houtkooper RH, Turkenburg M, Poll-The BT, Karall D, Perez-Cerda C, Morrone A, Malvagia S, Wanders RJ, Kulik W, Vaz FM. The enigmatic role of tafazzin in cardiolipin metabolism. *Biochim Biophys Acta.* 2009;1788:2003-14.
3. Bione S, D'Adamo P, Maestrini E, Gedeon AK, Bolhuis PA, Toniolo D. A novel X-linked gene, G4.5, is responsible for Barth syndrome. *Nat Genet.* 1996;12:385-9.
4. Bertero E, Kutschka I, Maack C, Dudek J. Cardiolipin remodeling in Barth syndrome and other hereditary cardiomyopathies. *Biochim Biophys Acta Mol Basis Dis.* 2020;1866:165803.
5. Zhang M, Mileykovskaya E, Dowhan W. Cardiolipin is essential for organization of complexes III and IV into a supercomplex in intact yeast mitochondria. *J Biol Chem.* 2005;280:29403-8.
6. Chatzisprou IA, Guerrero-Castillo S, Held NM, Ruiter JPN, Denis SW, L IJ, Wanders RJ, van Weeghel M, Ferdinandusse S, Vaz FM, et al. Barth syndrome cells display widespread remodeling of mitochondrial complexes without affecting metabolic flux distribution. *Biochim Biophys Acta Mol Basis Dis.* 2018;1864:3650-3658.
7. Dudek J, Cheng IF, Chowdhury A, Wozny K, Balleininger M, Reinhold R, Grunau S, Callegari S, Toischer K, Wanders RJ, et al. Cardiac-specific succinate dehydrogenase deficiency in Barth syndrome. *EMBO Mol Med.* 2016;8:139-54.
8. Dudek J, Cheng IF, Balleininger M, Vaz FM, Streckfuss-Bomeke K, Hubscher D, Vukotic M, Wanders RJ, Rehling P, Guan K. Cardiolipin deficiency affects respiratory chain function and organization in an induced pluripotent stem cell model of Barth syndrome. *Stem Cell Res.* 2013;11:806-19.
9. McKenzie M, Lazarou M, Thorburn DR, Ryan MT. Mitochondrial respiratory chain supercomplexes are destabilized in Barth Syndrome patients. *J Mol Biol.* 2006;361:462-9.
10. Gonzalez F, D'Aurelio M, Boutant M, Moustapha A, Puech JP, Landes T, Arnaune-Pelloquin L, Vial G, Taleux N, Slomianny C, et al. Barth syndrome: cellular compensation of mitochondrial dysfunction and apoptosis inhibition due to changes in cardiolipin remodeling linked to tafazzin (TAZ) gene mutation. *Biochim Biophys Acta.* 2013;1832:1194-206.
11. Wang G, McCain ML, Yang L, He A, Pasqualini FS, Agarwal A, Yuan H, Jiang D, Zhang D, Zangi L, et al. Modeling the mitochondrial cardiomyopathy of Barth syndrome with induced pluripotent stem cell and heart-on-chip technologies. *Nat Med.* 2014;20:616-23.
12. Chowdhury A, Aich A, Jain G, Wozny K, Luchtenborg C, Hartmann M, Bernhard O, Balleininger M, Alfar EA, Zieseniss A, et al. Defective Mitochondrial Cardiolipin Remodeling Dampens HIF-1alpha Expression in Hypoxia. *Cell Rep.* 2018;25:561-570 e6.
13. Nickel A, Kohlhaas M, Maack C. Mitochondrial reactive oxygen species production and elimination. *J Mol Cell Cardiol.* 2014;73C:26-33.
14. Acehan D, Vaz F, Houtkooper RH, James J, Moore V, Tokunaga C, Kulik W, Wansapura J, Toth MJ, Strauss A, et al. Cardiac and skeletal muscle defects in a mouse model of human Barth syndrome. *J Biol Chem.* 2011;286:899-908.

15. Huang Y, Powers C, Madala SK, Greis KD, Haffey WD, Towbin JA, Purevjav E, Javadov S, Strauss AW, Khuchua Z. Cardiac metabolic pathways affected in the mouse model of Barth syndrome. *PLoS One*. 2015;10:e0128561.
16. Kim J, Lee K, Fujioka H, Tandler B, Hoppel CL. Cardiac mitochondrial structure and function in tafazzin-knockdown mice. *Mitochondrion*. 2018;43:53-62.
17. Powers C, Huang Y, Strauss A, Khuchua Z. Diminished Exercise Capacity and Mitochondrial bc1 Complex Deficiency in Tafazzin-Knockdown Mice. *Front Physiol*. 2013;4:74.
18. Soustek MS, Falk DJ, Mah CS, Toth MJ, Schlame M, Lewin AS, Byrne BJ. Characterization of a transgenic short hairpin RNA-induced murine model of Tafazzin deficiency. *Hum Gene Ther*. 2011;22:865-71.
19. Bertero E, Maack C. Calcium Signaling and Reactive Oxygen Species in Mitochondria. *Circ Res*. 2018;122:1460-1478.
20. Saks V, Dzeja P, Schlattner U, Vendelin M, Terzic A, Wallimann T. Cardiac system bioenergetics: metabolic basis of the Frank-Starling law. *J Physiol*. 2006;571:253-73.
21. Cortassa S, Aon MA, Marbán E, Winslow RL, O'Rourke B. An integrated model of cardiac mitochondrial energy metabolism and calcium dynamics. *Biophys J*. 2003;84:2734-55.
22. Kembro JM, Aon MA, Winslow RL, O'Rourke B, Cortassa S. Integrating mitochondrial energetics, redox and ROS metabolic networks: a two-compartment model. *Biophys J*. 2013;104:332-43.
23. Nickel AG, von Hardenberg A, Hohl M, Löffler JR, Kohlhaas M, Becker J, Reil JC, Kazakov A, Bonnekoh J, Stadelmaier M, et al. Reversal of Mitochondrial Transhydrogenase Causes Oxidative Stress in Heart Failure. *Cell Metab*. 2015;22:472-84.
24. Kohlhaas M, Maack C. Adverse bioenergetic consequences of Na⁺-Ca²⁺ exchanger-mediated Ca²⁺ influx in cardiac myocytes. *Circulation*. 2010;122:2273-80.
25. Maack C, Cortassa S, Aon MA, Ganesan AN, Liu T, O'Rourke B. Elevated cytosolic Na⁺ decreases mitochondrial Ca²⁺ uptake during excitation-contraction coupling and impairs energetic adaptation in cardiac myocytes. *Circ Res*. 2006;99:172-82.
26. Kohlhaas M, Liu T, Knopp A, Zeller T, Ong MF, Böhm M, O'Rourke B, Maack C. Elevated cytosolic Na⁺ increases mitochondrial formation of reactive oxygen species in failing cardiac myocytes. *Circulation*. 2010;121:1606-13.
27. Liu T, Takimoto E, Dimaano VL, DeMazumder D, Kettlewell S, Smith G, Sidor A, Abraham TP, O'Rourke B. Inhibiting mitochondrial Na⁺/Ca²⁺ exchange prevents sudden death in a Guinea pig model of heart failure. *Circ Res*. 2014;115:44-54.
28. Dai DF, Johnson SC, Villarín JJ, Chin MT, Nieves-Cintrón M, Chen T, Marcinek DJ, Dorn GW, 2nd, Kang YJ, Prolla TA, et al. Mitochondrial oxidative stress mediates angiotensin II-induced cardiac hypertrophy and Galphaq overexpression-induced heart failure. *Circ Res*. 2011;108:837-46.
29. Dey S, DeMazumder D, Sidor A, Foster DB, O'Rourke B. Mitochondrial ROS Drive Sudden Cardiac Death and Chronic Proteome Remodeling in Heart Failure. *Circ Res*. 2018;123:356-371.
30. Dai DF, Hsieh EJ, Chen T, Menendez LG, Basisty NB, Tsai L, Beyer RP, Crispin DA, Shulman NJ, Szeto HH, et al. Global proteomics and pathway analysis of pressure-overload-induced heart failure and its attenuation by mitochondrial-targeted peptides. *Circ Heart Fail*. 2013;6:1067-76.

31. Dai DF, Chen T, Szeto H, Nieves-Cintron M, Kutayavin V, Santana LF, Rabinovitch PS. Mitochondrial targeted antioxidant Peptide ameliorates hypertensive cardiomyopathy. *J Am Coll Cardiol*. 2011;58:73-82.
32. Sabbah HN, Gupta RC, Kohli S, Wang M, Hachem S, Zhang K. Chronic Therapy With Elamipretide (MTP-131), a Novel Mitochondria-Targeting Peptide, Improves Left Ventricular and Mitochondrial Function in Dogs With Advanced Heart Failure. *Circ Heart Fail*. 2016;9:e002206.
33. Spencer CT, Byrne BJ, Bryant RM, Margossian R, Maisenbacher M, Breitenger P, Benni PB, Redfearn S, Marcus E, Cade WT. Impaired cardiac reserve and severely diminished skeletal muscle O₂ utilization mediate exercise intolerance in Barth syndrome. *Am J Physiol Heart Circ Physiol*. 2011;301:H2122-9.
34. Rigaud C, Lebre A-S, Touraine R, Beaupain B, Ottolenghi C, Chabli A, Ansquer H, Ozsahin H, Di Filippo S, De Lonlay P, et al. Natural history of Barth syndrome: a national cohort study of 22 patients. *Orphanet J Rare Dis*. 2013;8:70.
35. Kang S-L, Forsey J, Dudley D, Steward CG, Tsai-Goodman B. Clinical Characteristics and Outcomes of Cardiomyopathy in Barth Syndrome: The UK Experience. *Pediatr Cardiol*. 2016;37:167-176.
36. Spencer CT, Bryant RM, Day J, Gonzalez IL, Colan SD, Thompson WR, Berthy J, Redfearn SP, Byrne BJ. Cardiac and clinical phenotype in Barth syndrome. *Pediatrics*. 2006;118:e337-46.
37. Roberts AE, Nixon C, Steward CG, Gauvreau K, Maisenbacher M, Fletcher M, Geva J, Byrne BJ, Spencer CT. The Barth Syndrome Registry: Distinguishing disease characteristics and growth data from a longitudinal study. *Am J Med Genet A*. 2012;158A:2726-2732.
38. Spencer CT, Byrne BJ, Gewitz MH, Wechsler SB, Kao AC, Gerstenfeld EP, Merliss AD, Carboni MP, Bryant RM. Ventricular Arrhythmia in the X-linked Cardiomyopathy Barth Syndrome. *Pediatr Cardiol*. 2005;26:632-637.
39. Bers DM. *Excitation-contraction coupling and cardiac contractile force*. 2nd ed. Dordrecht, The Netherlands: Kluwer Academic Publisher; 2001.
40. Bers DM. Cardiac excitation-contraction coupling. *Nature*. 2002;415:198-205.
41. Eisner DA, Caldwell JL, Kistamas K, Trafford AW. Calcium and Excitation-Contraction Coupling in the Heart. *Circ Res*. 2017;121:181-195.
42. Brenner B. Effect of Ca²⁺ on cross-bridge turnover kinetics in skinned single rabbit psoas fibers: implications for regulation of muscle contraction. *Proc Natl Acad Sci U S A*. 1988;85:3265-9.
43. Sequeira V, Najafi A, McConnell M, Fowler ED, Bollen IA, Wust RC, dos Remedios C, Helmes M, White E, Stienen GJ, et al. Synergistic role of ADP and Ca(2+) in diastolic myocardial stiffness. *J Physiol*. 2015;593:3899-916.
44. Johnson JM, Ferrara PJ, Verkerke ARP, Coleman CB, Wentzler EJ, Neuffer PD, Kew KA, de Castro Bras LE, Funai K. Targeted overexpression of catalase to mitochondria does not prevent cardioskeletal myopathy in Barth syndrome. *J Mol Cell Cardiol*. 2018;121:94-102.
45. Pan X, Liu J, Nguyen T, Liu C, Sun J, Teng Y, Fergusson MM, Rovira, II, Allen M, Springer DA, et al. The physiological role of mitochondrial calcium revealed by mice lacking the mitochondrial calcium uniporter. *Nat Cell Biol*. 2013;15:1464-72.
46. Raffaello A, De Stefani D, Sabbadin D, Teardo E, Merli G, Picard A, Checchetto V, Moro S, Szabo I, Rizzuto R. The mitochondrial calcium uniporter is a multimer that can include a dominant-negative pore-forming subunit. *The EMBO journal*. 2013;32:2362-76.

47. Lambert JP, Luongo TS, Tomar D, Jadiya P, Gao E, Zhang X, Lucchese AM, Kolmetzky DW, Shah NS, Elrod JW. MCUB Regulates the Molecular Composition of the Mitochondrial Calcium Uniporter Channel to Limit Mitochondrial Calcium Overload During Stress. *Circulation*. 2019;140:1720-1733.
48. Bashir A, Bohnert KL, Reeds DN, Peterson LR, Bittel AJ, de Las Fuentes L, Pacak CA, Byrne BJ, Cade WT. Impaired cardiac and skeletal muscle bioenergetics in children, adolescents, and young adults with Barth syndrome. *Physiol Rep*. 2017;5:e13130.
49. Williams GS, Boyman L, Chikando AC, Khairallah RJ, Lederer WJ. Mitochondrial calcium uptake. *Proc Natl Acad Sci U S A*. 2013;110:10479-86.
50. Fieni F, Lee SB, Jan YN, Kirichok Y. Activity of the mitochondrial calcium uniporter varies greatly between tissues. *Nat Commun*. 2012;3:1317.
51. Brandes R, Bers DM. Intracellular Ca²⁺ increases the mitochondrial NADH concentration during elevated work in intact cardiac muscle. *Circ Res*. 1997;80:82-7.
52. Fujikawa Y, Roma LP, Sobotta MC, Rose AJ, Diaz MB, Locatelli G, Breckwoldt MO, Misgeld T, Kerschensteiner M, Herzig S, et al. Mouse redox histology using genetically encoded probes. *Sci Signal*. 2016;9:rs1-rs1.
53. Nichols CG, Lederer WJ. Adenosine triphosphate-sensitive potassium channels in the cardiovascular system. *Am J Physiol Heart Circ Physiol*. 1991;261:H1675-H1686.
54. Sasaki N, Sato T, Marbán E, O'Rourke B. ATP consumption by uncoupled mitochondria activates sarcolemmal K(ATP) channels in cardiac myocytes. *Am J Physiol Heart Circ Physiol*. 2001;280:H1882-8.
55. Hiraoka M, Fan Z, Furukawa T, Nakayama K, Sawanobori T. Activation and reactivation of the ATP-sensitive K⁺ channel of the heart can be modified by drugs. *Cardiovasc Drugs Ther*. 1993;7:593-598.
56. Liu Y, Ren G, O'Rourke B, Marbán E, Seharaseyon J. Pharmacological comparison of native mitochondrial K(ATP) channels with molecularly defined surface K(ATP) channels. *Mol Pharmacol*. 2001;59:225-30.
57. Prosser BL, Ward CW, Lederer WJ. X-ROS signaling: rapid mechano-chemo transduction in heart. *Science*. 2011;333:1440-5.
58. Helmes M, Najafi A, Palmer BM, Breel E, Rijnveld N, Iannuzzi D, van der Velden J. Mimicking the cardiac cycle in intact cardiomyocytes using diastolic and systolic force clamps; measuring power output. *Cardiovasc Res*. 2016;111:66-73.
59. Bers DM, Bassani RA, Bassani JW, Baudet S, Hryshko LV. Paradoxical twitch potentiation after rest in cardiac muscle: increased fractional release of SR calcium. *J Mol Cell Cardiol*. 1993;25:1047-57.
60. Luongo TS, Lambert JP, Yuan A, Zhang X, Gross P, Song J, Shanmughapriya S, Gao E, Jain M, Houser SR, et al. The Mitochondrial Calcium Uniporter Matches Energetic Supply with Cardiac Workload during Stress and Modulates Permeability Transition. *Cell Rep*. 2015;12:23-34.
61. Huke S, Venkataraman R, Faggioni M, Bennuri S, Hwang HS, Baudenbacher F, Knollmann BC. Focal energy deprivation underlies arrhythmia susceptibility in mice with calcium-sensitized myofilaments. *Circ Res*. 2013;112:1334-44.
62. Thompson WR, DeCroes B, McClellan R, Rubens J, Vaz FM, Kristaponis K, Avramopoulos D, Vernon HJ. New targets for monitoring and therapy in Barth syndrome. *Genet Med*. 2016;18:1001-1010.

63. Abudiab MM, Redfield MM, Melenovsky V, Olson TP, Kass DA, Johnson BD, Borlaug BA. Cardiac output response to exercise in relation to metabolic demand in heart failure with preserved ejection fraction. *Eur J Heart Fail*. 2013;15:776-85.
64. Borlaug BA, Melenovsky V, Russell SD, Kessler K, Pacak K, Becker LC, Kass DA. Impaired chronotropic and vasodilator reserves limit exercise capacity in patients with heart failure and a preserved ejection fraction. *Circulation*. 2006;114:2138-47.
65. Kraigher-Krainer E, Shah AM, Gupta DK, Santos A, Claggett B, Pieske B, Zile MR, Voors AA, Lefkowitz MP, Packer M, et al. Impaired systolic function by strain imaging in heart failure with preserved ejection fraction. *J Am Coll Cardiol*. 2014;63:447-56.
66. Ferreira C, Thompson R, Vernon H. Barth Syndrome. In: M. P. Adam, H. H. Ardinger, R. A. Pagon, S. E. Wallace, L. J. H. Bean, K. Stephens and A. Amemiya, eds. *GeneReviews*((R)) Seattle (WA); 2014.
67. Watkins H, Ashrafian H, Redwood C. Inherited cardiomyopathies. *N Engl J Med*. 2011;364:1643-56.
68. Hobai IA, O'Rourke B. Decreased sarcoplasmic reticulum calcium content is responsible for defective excitation-contraction coupling in canine heart failure. *Circulation*. 2001;103:1577-84.
69. Piacentino V, Weber CR, Chen X, Weisser-Thomas J, Margulies KB, Bers DM, Houser SR. Cellular Basis of Abnormal Calcium Transients of Failing Human Ventricular Myocytes. *Circ Res*. 2003;92:651-658.
70. Braun JL, Hamstra SI, Messner HN, Fajardo VA. SERCA2a tyrosine nitration coincides with impairments in maximal SERCA activity in left ventricles from tafazzin-deficient mice. *Physiol Rep*. 2019;7:e14215.
71. Wang S, Li Y, Xu Y, Ma Q, Lin Z, Schlame M, Bezzerides VJ, Strathdee D, Pu WT. AAV Gene Therapy Prevents and Reverses Heart Failure in a Murine Knockout Model of Barth Syndrome. *Circ Res*. 2020;126:1024-1039.
72. Liu X, Wang S, Guo X, Li Y, Ogurlu R, Lu F, Prondzynski M, de la Serna Buzon S, Ma Q, Zhang D, et al. Increased Reactive Oxygen Species-Mediated Ca(2+)/Calmodulin-Dependent Protein Kinase II Activation Contributes to Calcium Handling Abnormalities and Impaired Contraction in Barth Syndrome. *Circulation*. 2021;143:1894-1911.
73. Ghosh S, Basu Ball W, Madaris TR, Srikantan S, Madesh M, Mootha VK, Gohil VM. An essential role for cardiolipin in the stability and function of the mitochondrial calcium uniporter. *Proc Natl Acad Sci U S A*. 2020;117:16383-16390.
74. Stefanyk LE, Coverdale N, Roy BD, Peters SJ, LeBlanc PJ. Skeletal muscle type comparison of subsarcolemmal mitochondrial membrane phospholipid fatty acid composition in rat. *J Membr Biol*. 2010;234:207-15.
75. Fajardo VA, Mikhaeil JS, Leveille CF, Saint C, LeBlanc PJ. Cardiolipin content, linoleic acid composition, and tafazzin expression in response to skeletal muscle overload and unload stimuli. *Sci Rep*. 2017;7:2060.
76. Cortassa S, Aon MA, O'Rourke B, Jacques R, Tseng HJ, Marbán E, Winslow RL. A computational model integrating electrophysiology, contraction, and mitochondrial bioenergetics in the ventricular myocyte. *Biophys J*. 2006;91:1564-89.
77. Aon MA, Cortassa S, O'Rourke B. Redox-optimized ROS balance: a unifying hypothesis. *Biochim Biophys Acta*. 2010;1797:865-77.
78. Goncalves RLS, Schlame M, Bartelt A, Brand MD, Hotamışlıgil GS. Cardiolipin deficiency in Barth syndrome is not associated with increased superoxide/H(2) O(2) production in heart and skeletal muscle mitochondria. *FEBS Lett*. 2020. doi: 10.1002/1873-3468.13973

79. Yun J, Finkel T. Mitohormesis. *Cell Metab.* 2014;19:757-66.
80. Ma Q. Role of nrf2 in oxidative stress and toxicity. *Annu Rev Pharmacol Toxicol.* 2013;53:401-26.
81. He Q, Harris N, Ren J, Han X. Mitochondria-targeted antioxidant prevents cardiac dysfunction induced by tafazzin gene knockdown in cardiac myocytes. *Oxid Med Cell Longev.* 2014;2014:654198.
82. Saric A, Andreau K, Armand AS, Møller IM, Petit PX. Barth Syndrome: From Mitochondrial Dysfunctions Associated with Aberrant Production of Reactive Oxygen Species to Pluripotent Stem Cell Studies. *Front Genet.* 2015;6:359.
83. Schober T, Huke S, Venkataraman R, Gryshchenko O, Kryshtal D, Hwang HS, Baudenbacher FJ, Knollmann BC. Myofilament Ca sensitization increases cytosolic Ca binding affinity, alters intracellular Ca homeostasis, and causes pause-dependent Ca-triggered arrhythmia. *Circ Res.* 2012;111:170-9.
84. Denton RM, McCormack JG. Ca²⁺ transport by mammalian mitochondria and its role in hormone action. *Am J Physiol.* 1985;249:E543-54.
85. Balaban RS. Cardiac energy metabolism homeostasis: role of cytosolic calcium. *J Mol Cell Cardiol.* 2002;34:1259-71.
86. Desai KH, Sato R, Schauble E, Barsh GS, Kobilka BK, Bernstein D. Cardiovascular indexes in the mouse at rest and with exercise: new tools to study models of cardiac disease. *Am J Physiol.* 1997;272:H1053-61.
87. Chapman CB, Fisher JN, Sproule BJ. Behavior of stroke volume at rest and during exercise in human beings. *J Clin Invest.* 1960;39:1208-13.
88. Taivassalo T, Dysgaard Jensen T, Kennaway N, DiMauro S, Vissing J, Haller RG. The spectrum of exercise tolerance in mitochondrial myopathies: a study of 40 patients. *Brain.* 2003;126:413-423.
89. Liu T, Brown DA, O'Rourke B. Role of mitochondrial dysfunction in cardiac glycoside toxicity. *J Mol Cell Cardiol.* 2010;49:728-36.
90. Green EM, Wakimoto H, Anderson RL, Evanchik MJ, Gorham JM, Harrison BC, Henze M, Kawas R, Oslob JD, Rodriguez HM, et al. A small-molecule inhibitor of sarcomere contractility suppresses hypertrophic cardiomyopathy in mice. *Science.* 2016;351:617-21.
91. Baartscheer A, Schumacher CA, Wüst RC, Fiolet JW, Stienen GJ, Coronel R, Zuurbier CJ. Empagliflozin decreases myocardial cytoplasmic Na⁽⁺⁾ through inhibition of the cardiac Na⁽⁺⁾/H⁽⁺⁾ exchanger in rats and rabbits. *Diabetologia.* 2017;60:568-573.
92. Streckfuss-Bomeke K, Wolf F, Azizian A, Stauske M, Tiburcy M, Wagner S, Hubscher D, Dressel R, Chen S, Jende J, et al. Comparative study of human-induced pluripotent stem cells derived from bone marrow cells, hair keratinocytes, and skin fibroblasts. *Eur Heart J.* 2013;34:2618-29.
93. Lian X, Zhang J, Azarin SM, Zhu K, Hazeltine LB, Bao X, Hsiao C, Kamp TJ, Palecek SP. Directed cardiomyocyte differentiation from human pluripotent stem cells by modulating Wnt/beta-catenin signaling under fully defined conditions. *Nat Protoc.* 2013;8:162-75.
94. Tohyama S, Hattori F, Sano M, Hishiki T, Nagahata Y, Matsuura T, Hashimoto H, Suzuki T, Yamashita H, Satoh Y, et al. Distinct metabolic flow enables large-scale purification of mouse and human pluripotent stem cell-derived cardiomyocytes. *Cell Stem Cell.* 2013;12:127-37.
95. Mela L, Seitz S. Isolation of mitochondria with emphasis on heart mitochondria from small amounts of tissue. *Methods Enzymol.* 1979;55:39-46.

96. Chappell JB, Perry SV. Biochemical and osmotic properties of skeletal muscle mitochondria. *Nature*. 1954;173:1094-5.
97. Ryan MT, Voos W, Pfanner N. Assaying protein import into mitochondria. *Methods Cell Biol*. 2001;65:189-215.
98. Heiberg E, Sjogren J, Ugander M, Carlsson M, Engblom H, Arheden H. Design and validation of Segment--freely available software for cardiovascular image analysis. *BMC Med Imaging*. 2010;10:1.
99. Seeland U, Selejan S, Engelhardt S, Muller P, Lohse MJ, Bohm M. Interstitial remodeling in beta1-adrenergic receptor transgenic mice. *Basic Res Cardiol*. 2007;102:183-93.



Circulation

Figure Legends

Figure 1. *Taz*-KD Cardiomyopathy is Reminiscent of Heart Failure with Preserved Ejection Fraction

A, Representative image of one 50-week-old (w/o) *Taz*-KD mouse compared with a WT littermate. **B**, Body weight and heart weight/tibia length ratio of *Taz*-KD mice and WT littermates at 10 weeks (WT n=5; *Taz*-KD, n=6), 20 weeks (n=10/13) and 50 weeks (n=16/12), respectively. **D-I**, Invasive determination of left ventricular end-diastolic volume (LVEDV; **D**), ejection fraction (LVEF; **E**), maximal rate of pressure rise (dP/dt_{max} ; **F**) and fall (dP/dt_{min} ; **G**), and end-systolic (ESPVR; **H**) and end-diastolic pressure-volume relationship (EDPVR; **I**) in WT (n=19) and *Taz*-KD mice (n=16), respectively. **J-L**, Magnetic resonance imaging-derived assessment of LVEF (**J**), cardiac output (**K**), and LVEDV (**L**), between 10 and 50 weeks, respectively (10 to 20 weeks: WT n=5, *Taz*-KD n=6; 50 weeks: n=16/12). **M**, Cardiac mRNA levels of atrial natriuretic peptide (*Anp*) and connective tissue growth factor (*Ctgf*) normalized to WT in 10, 20, and 50 w/o mice (WT, n=4; *Taz*-KD, n=3). **N**, Representative Doppler echocardiography images of mitral inflow velocity in 50 w/o mice. **O**, Representative histology image of LV myocardium from 50 w/o mice stained with Picrosirius red to detect interstitial fibrosis. **P**, Quantification of LV interstitial fibrosis in 50 w/o mice (n=6 per group).

Data represent mean \pm SEM (indicated by error bars); n-numbers are indicated as numbers of hearts or animals; statistical significance was determined by unpaired Student's t-test in **B-I** and **P** and for the 50 week group in **J** to **L**; and by 2-way ANOVA followed by Bonferroni post-test in **J** to **L**, age groups 10 to 20 weeks.

indicates $p < 0.05$ with 2-way ANOVA;

*: $p < 0.05$ with Bonferroni post-test;

†, ‡, ††, †††: $p < 0.05$, $p < 0.01$, $p < 0.001$, $p < 0.0001$ with unpaired Student's t-test.

Figure 2. Alterations of Excitation-Contraction Coupling in *Taz*-KD Versus WT Cardiac Myocytes

For experiments shown in **A** to **H**, isolated cardiac myocytes isolated from 10 w/o WT or *Taz*-KD mice were field-stimulated at 0.5 Hz for 120 s, superfused with isoproterenol (Iso; 30 nM), and stimulation frequency was increased from 0.5 Hz to 5 Hz for 180 s. **A**, Averaged original traces of sarcomere length of cardiac myocytes loaded with the cell-permeant ratiometric Ca^{2+} indicator Indo-1 AM (n=22/3 per group). Systolic and diastolic sarcomere length (**B**) and fractional sarcomere shortening of unloaded cardiac myocytes (**C**), respectively (WT n=38/3, *Taz*-KD n=28/3). **D**, Time to 50% sarcomere re-lengthening of cardiac myocytes from 10 and 50 w/o mice (10 weeks: WT n=38/3, *Taz*-KD n=28/3; 50 weeks: WT n=30/4, *Taz*-KD n=26/4). **E-G**, Averaged original traces of cytosolic Ca^{2+} transients ($[\text{Ca}^{2+}]_c$; **E**), systolic and diastolic cytosolic Ca^{2+} ($[\text{Ca}^{2+}]_c$; **F**), and time to $[\text{Ca}^{2+}]_c$ decay (**G**) of intact cardiac myocytes loaded with the cell-permeant ratiometric Ca^{2+} indicator Indo-1 AM (n=22/3 per group). **H**, $[\text{Ca}^{2+}]_c$ levels plotted against sarcomere length. Data are extracted from the experiments shown in **E** to **G** (n=22/3 per group). In the experiments shown in **I** to **P**, caffeine (10 mM) pulses were applied to cardiac myocytes loaded with Indo-1 after 120 s of 0.5 Hz or combined Iso/5 Hz stimulation (0.5 Hz: WT n=24/2, *Taz*-KD; n=27/2; Iso/5 Hz: WT n=12/2, *Taz*-KD n=16/2). **I**, Averaged original traces of cytosolic Ca^{2+} transients ($[\text{Ca}^{2+}]_c$). **J**, Caffeine-induced increase in $[\text{Ca}^{2+}]_c$, indicating SR Ca^{2+} load after 0.5 Hz or Iso/5 Hz stimulation. **K**, Fractional Ca^{2+} release from the SR calculated as the % amplitude of steady-state Ca^{2+} transients compared with the caffeine-induced increase in $[\text{Ca}^{2+}]_c$,

respectively. **L**, Diastolic $[Ca^{2+}]_c$ during steady-state 0.5 Hz or Iso/5 Hz stimulation. **M**, Maximal cellular and SR Ca^{2+} load during pacing at 0.5 Hz or Iso/5 Hz, reflecting the maximal $[Ca^{2+}]_c$ after the caffeine pulse after the respective conditions. **N**, Net change of total cellular and SR Ca^{2+} load induced by Iso/5 Hz stimulation, calculated as the difference between the values at 0.5 Hz and Iso/5 Hz as indicated in **M**. **O**, Kinetics of $[Ca^{2+}]_c$ decay of steady-state $[Ca^{2+}]_c$ transients during 0.5 Hz or Iso/5 Hz stimulation, reporting largely Ca^{2+} removal by the SR Ca^{2+} ATPase (SERCA). **P**, Kinetics of $[Ca^{2+}]_c$ decay after caffeine pulses after 0.5 Hz or Iso/5 Hz stimulation as an indicator of Ca^{2+} removal by the sarcolemmal Na^+/Ca^{2+} exchanger (NCX). In the experiments shown in **Q** and **R**, permeabilized cardiac myocytes were used (WT n=18/4, *Taz*-KD n=15/4) and intracellular Ca^{2+} concentrations defined to assess Ca^{2+} -dependent force generation of myofilaments. **Q**, Force- Ca^{2+} relations of permeabilized loaded cardiac myocytes. **R**, Normalized rate constant of tension redevelopment (k_{TR}) as a function of Ca^{2+} -activated isometric force.

Data represent mean \pm SEM [indicated by dotted lines in **A** and **H**, by error bars in other panels]; n-numbers are indicated as numbers of cardiac myocytes / animals; statistical significance was determined by 2-way ANOVA followed by Bonferroni post-test.

indicates $p < 0.05$ with 2-way ANOVA;

*, **, ***, *****: $p < 0.05$, $p < 0.01$, $p < 0.001$, $p < 0.0001$ with Bonferroni post-test.

Figure 3. Structural Remodeling of The Respiratory Chain Impairs Respiration, but Does Not Increase ROS Emission in Cardiac Mitochondria of *Taz*-KD Mice

A, Blue native gel electrophoresis (BN-PAGE) analysis of isolated heart mitochondria from 10 and 50 w/o mice, respectively. Western blot and immunodecoration performed with antibodies

against the following proteins (from left to right): NADH dehydrogenase 1 β subcomplex subunit 8 (NDUFB8) of complex I, the complex III component Rieske (UQCRFS1), and the cytochrome *c* oxidase (complex IV) subunit 5a (COX5A). **B**, O₂ consumption of isolated cardiac mitochondria from 10 w/o mice supplied with pyruvate and malate (5/5 mM) as substrates in the absence (State 2) and presence of different ADP concentrations (State 3). The complex V inhibitor oligomycin was added to inhibit phosphorylation-coupled respiration (State 4; n=6 per group). **C**, Superoxide ($\cdot\text{O}_2^-$) formation of isolated cardiac mitochondria from 10 w/o mice supplied with pyruvate and malate (5/5 mM) and different ADP concentrations. The protonophore 2,4-dinitrophenol (DNP) and the complex III inhibitor antimycin A (AntiA) were added to uncouple respiration from ADP phosphorylation and as a positive control inducing $\cdot\text{O}_2^-$ formation at complex III, respectively (n=3 per group). **D**, Hydrogen peroxide (H₂O₂) emission of isolated cardiac mitochondria from 10 w/o mice supplied with pyruvate and malate (5/5 mM) and different ADP concentrations. The complex III inhibitor antimycin A (AntiA) was added as a positive control (n=5 per group). **E**, State 3 (ADP 1 mM) O₂ consumption of isolated cardiac mitochondria from 10, 20, and 50 w/o mice (10 weeks: n=6 per group; 20 weeks: WT=4, *Taz*-KD=3; 50 weeks: WT=7, *Taz*-KD=6). **F**, State 3 (ADP 1 mM) $\cdot\text{O}_2^-$ formation of isolated cardiac mitochondria from 10 and 50 w/o mice (n=3 per group and age). **G**, State 3 (ADP 1 mM) H₂O₂ emission of isolated cardiac mitochondria from 10, 20, and 50 w/o mice (10 weeks: n=5 per group; 20 weeks: WT=4, *Taz*-KD=3; 50 weeks: n=5 per group). Data shown in **E**, **F** and **G** summarize the results shown in **B**, **C** and **D** together with those shown in **Figure IX** in the Supplement.

Data represent mean \pm SEM (indicated by error bars); n-numbers are indicated as numbers of hearts or animals; statistical significance was determined by 2-way ANOVA followed by Bonferroni post-test.

indicates $p < 0.05$ with 2-way ANOVA;

, *: $p < 0.01$, $p < 0.0001$ with Bonferroni post-test.

Figure 4. Loss of The Mitochondrial Ca^{2+} Uniporter Abrogates Ca^{2+} Uptake Into Cardiac Mitochondria of *Taz*-Kd Mice

A, Ca^{2+} retention capacity of isolated cardiac mitochondria from 10 w/o mice exposed to repetitive 10 μM Ca^{2+} pulses at 120 s intervals. Extramitochondrial Ca^{2+} was monitored with CalciumGreen 5N. Cyclosporine A (CsA) was added to prevent mitochondrial permeability transition (dashed traces; WT n=5, *Taz*-KD n=4). **B**, BN-PAGE analysis of MCUa in cardiac mitochondria of 3 independent pairs of 10 w/o *Taz*-KD, *Mcu* knockout (*Mcu*-KO), and WT littermates (*Taz*-WT and *Mcu*-WT, respectively). MCU-specific bands are indicated with stars (*), non-specific bands with circles ($^{\circ}$). **C**, Representative western blot and quantification of MCU complex subunits MCUa, MCUb, EMRE, MCUR1, MICU1, and MICU2 in hearts of 10 w/o *Taz*-KD mice (n=6 per group). Data are presented as intensity optical density (IOD) of the specific band to IOD of cytochrome oxidase subunit 4 (COX4). **D**, Cardiac *Mcu*a mRNA levels in 10 w/o mice (n=7 per group). **E**, Western blot and quantification of MCUa, voltage-dependent anion-selective channel 3 (VDAC3), NADH dehydrogenase 1 β subcomplex subunit 8 (NDUFB8), and mitochondrial $\text{H}^{+}/\text{Ca}^{2+}$ exchanger (LETM1) levels in iPSC-derived cardiac myocytes obtained from a patient with Barth syndrome (indicated as TAZ10) and one healthy control.

Data represent mean \pm SEM (indicated by dotted lines in **A**, by error bars in other panels); n-numbers are indicated as numbers of hearts or animals; statistical significance was determined unpaired Student t-test.

Figure 5. Defective Mitochondrial Ca²⁺ Uptake Provokes Mitochondrial Oxidation and Cellular Arrhythmias During Workload Transitions in *Taz*-Kd Cardiac Myocytes

For experiments shown in **A** to **G**, isolated cardiac myocytes from 10 w/o WT and *Taz*-KD mice were subjected to the same experimental protocol described for **Figure 2A-H** and cytosolic and mitochondrial Ca²⁺ concentrations ([Ca²⁺]_c and [Ca²⁺]_m, respectively) were determined in the same cells. The gray-shaded area in the graphs indicates 5 Hz stimulation. **A-C**, Cytosolic Ca²⁺ concentration (**A**), averaged original traces of mitochondrial Ca²⁺ transients (**B**) and diastolic mitochondrial Ca²⁺ concentration (**C**) in the same patch-clamped cardiac myocytes, respectively (WT n=15/8, *Taz*-KD n=13/7). **D-E**, Autofluorescence of NAD(P)H and FAD (**D**) and the ratio of NAD(P)H/FAD (**E**) calculated from the data in **D** as an indicator of the mitochondrial pyridine nucleotide redox state in intact cardiac myocytes (WT n=29/3, *Taz*-KD n=24/3). **F**, Mitochondrial membrane potential ($\Delta\Psi_m$) determined by TMRM in WT (n=20/3) and *Taz*-KD myocytes (n=18/3). **G**, Two representative traces of sarcomere shortening in a WT and *Taz*-KD myocyte, respectively. Cells were captured during 0.5 Hz stimulation after the Iso/5 Hz stress protocol. In WT, regular systolic sarcomere shortening in response to the triggered field stimulation pulses can be observed, while in the *Taz*-KD myocytes, autonomic sarcomere shortenings uncoupled from electrical stimulation occur, categorized as “cellular arrhythmias”. **H**, Percentage of cardiac myocytes showing non-stimulated sarcomere shortenings (“cellular arrhythmias” as indicated in **G**) after Iso/5 Hz at 10, 20, and 50 weeks of age, respectively. Data were extracted from

experiments in **D** and **Figure XII** in the Supplement (10 weeks: WT n=29/3, *Taz*-KD n=24/3; 20 weeks: WT n=13/3, *Taz*-KD n=24/3; 50 weeks: WT n=30/4, *Taz*-KD n=26/4).

In the experiments shown in **I** and **J**, cardiac myocytes from 20 w/o mice were superfused with the mitochondrial Na⁺/Ca²⁺ exchanger (NCLX) inhibitor CGP-37157 (CGP; 10 μM) or vehicle (DMSO) for 240 s before being subjected to Iso/5 Hz stimulation for 180 s (n=12/3 per group). **I**, Normalized NAD(P)H/FAD ratio of intact cardiac myocytes from 20 w/o *Taz*-KD mice. **J**, Percentage of cardiac myocytes showing non-stimulated sarcomere shortenings (“cellular arrhythmias”) after Iso/5 Hz and treatment with CGP or vehicle (Con) from the experiment shown in **I**.

Data represent mean ± SEM (indicated by dotted lines in **A**, **C**, **D**, **E** and **H**); n-numbers are indicated as numbers of cardiac myocytes / animals; statistical significance was determined by 2-way ANOVA followed by Bonferroni post-test in **A**, **C**, **D**, **E**, and **H**, by Fisher’s exact test in **G**, and by Chi-square test in **I**.

indicates $p < 0.05$ with 2-way ANOVA;

*, **: $p < 0.05$, $p < 0.01$ with Bonferroni post-test;

§, §§, §§§, §§§§: $p < 0.05$, $p < 0.01$, $p < 0.001$, $p < 0.0001$ with Fisher’s exact test in **G**, Chi-square test in **I**.

Figure 6. Mitochondrial ROS Emission is Prevented by Upregulation of ROS-Detoxifying Capacity in Young *Taz*-KD Cardiac Myocytes

A, ROS emission determined with the fluorescent indicator DCF in intact cardiac myocytes from 10 w/o mice subjected to the same experimental protocol described for **Figures 2A-H** and **5A-G**

(WT n=40/4, *Taz*-KD n=26/4). Representative measurement (**B**) and quantification of DCF fluorescence (**C**) in response to superfusion with 1 mM H₂O₂ of intact cardiac myocytes from 10 w/o mice (WT n=40/4, *Taz*-KD n=26/4). **D**, Protein levels of cardiac catalase (CAT), glutathione peroxidase 1 (GPX1), peroxiredoxin (PRDX) 1, 2, and 3, and superoxide dismutase (SOD) 1 and 2 related to the expression of GAPDH and normalized to WT in 10, 20, and 50 w/o mice (n=6 per group for 10 and 50 w/o; WT n=4, *Taz*-KD n=3 for 20 w/o). Representative blots are from 10 w/o hearts. **E**, Representative ratiometric image (excitation: 405/488 nm; emission: 500-530 nm) of mito-roGFP2-Orp1/WT (left) and mito-roGFP2-Orp1/*Taz*-KD (right) heart histology slices at 20 (top row) or 50 weeks (bottom row). **F**, Normalized fold change in ratio (%) of the redox state of the mito-roGFP2-Orp1 sensor in the hearts of 20 and 50 w/o mito-roGFP2-Orp1/WT and mito-roGFP2-Orp1/*Taz*-KD mice (20 weeks: n=4 per group; 50 weeks: WT n=6, *Taz*-KD n=5). **G**, Staining of 8-hydroxy-2'-deoxyguanosine (8-OHdG) in WT and *Taz*-KD hearts (n=6 per group). **H**, Activity of aconitase in hearts of WT (n=12) and *Taz*-KD (n=9) mice. Data represent mean \pm SEM (indicated by dotted lines in **A**, by error bars in other panels); n-numbers are indicated as numbers of cardiac myocytes / animals in **A** and **C** and as number of hearts or animals for **D** to **H**; statistical significance was determined by 2-way ANOVA followed by Bonferroni post-test in **A**, and by unpaired Student t-test in **C** to **H**.

†, ‡: $p < 0.05$, $p < 0.01$ with unpaired Student t-test.

Figure 7. Defective Inotropic Reserve and Slowed Intraventricular Conduction in *Taz*-KD Hearts

A, Fractional sarcomere shortening of isolated cardiac myocytes from 20 w/o WT and *Taz*-KD mice. Cardiac myocytes were field-stimulated at 0.5 Hz and superfused with the K_{ATP} channel sensitizer pinacidil (red trace; WT n=8/2, *Taz*-KD n=6/2), the K_{ATP} channel inhibitor HMR (blue; WT n=8/2, *Taz*-KD n=7/2), or vehicle (black; WT n=8/2, *Taz*-KD n=7/2) for 240 s before being subjected to Iso/5 Hz stimulation for 180 s. **B**, Representative trace of force developed by one isolated cardiac myocyte pre-stretched with glass fibers to exert isometric contractions demonstrating the preload-dependent potentiation of force by the Frank-Starling mechanism. **C**, Representative traces of force development of isolated pre-stretched cardiac myocytes from 20 w/o mice subjected to the protocol shown in **B**. Averaged original traces (**D**) and quantification of force (**E**) developed by isolated cardiac myocytes subjected to the protocol shown in **B** (n=2/2 per group). **F-H**, Heart rate (**F**), maximal rate of pressure rise (dp/dt_{max} ; **G**), and left ventricular stroke volume (**H**) in anaesthetized WT and *Taz*-KD mice in response to intravenous infusion with dobutamine at 10 and 40 ng/g \times min, after injection of either vehicle (Veh.; WT, n=8; *Taz*-KD, n=8) or CGP-37157 (CGP; 0.02 mg/kg; WT, n=8; *Taz*-KD, n=12). **I**, Correlation of MCU protein levels and LV stroke volume at 40 ng/g \times min after injection of CGP-37157, respectively. **J**, Original traces of surface ECG recordings in WT and *Taz*-KD mice after injection of dobutamine (10 ng/g \times min) and either vehicle (above) or CGP-37157 (below). **K**, Cumulative analyses of QRS duration in WT (Veh., n=6; CGP, n=5) or *Taz*-KD mice (Veh., n=6; CGP, n=5) before (baseline, BL) and after injection of either vehicle (+Veh.) or CGP-37157 (+CGP), and then dobutamine (+Dob; 10 ng/g \times min).

Data represent mean \pm SEM (indicated by error bars); n-numbers are indicated as numbers of cardiac myocytes / animals; statistical significance was determined by repeated measures ANOVA for **A** and by 2-way ANOVA followed by Bonferroni post-test for **E-H** and **K**.

$p < 0.05$ with 2-way ANOVA;

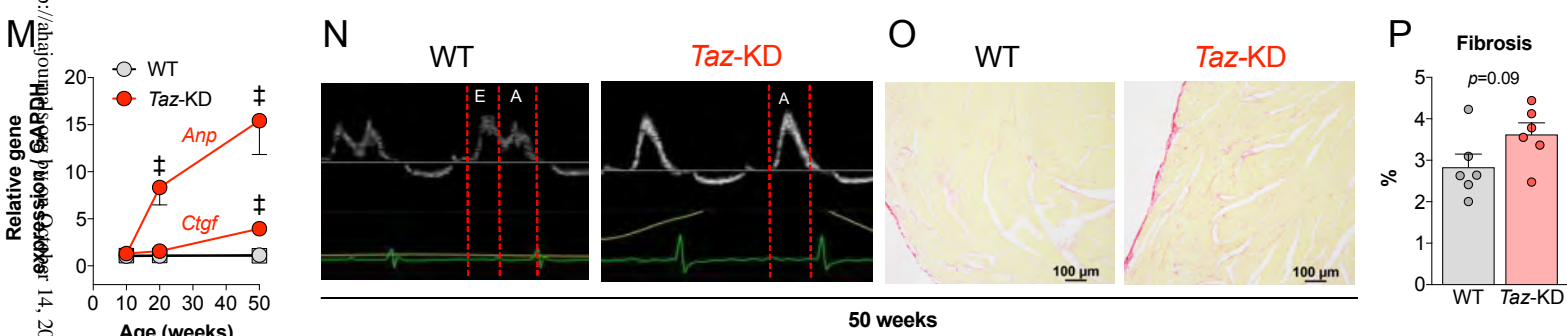
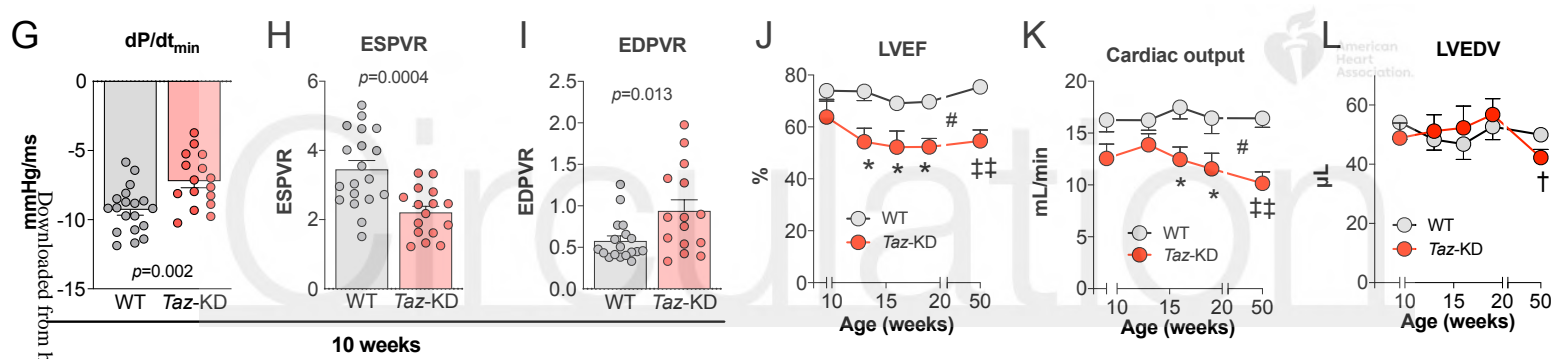
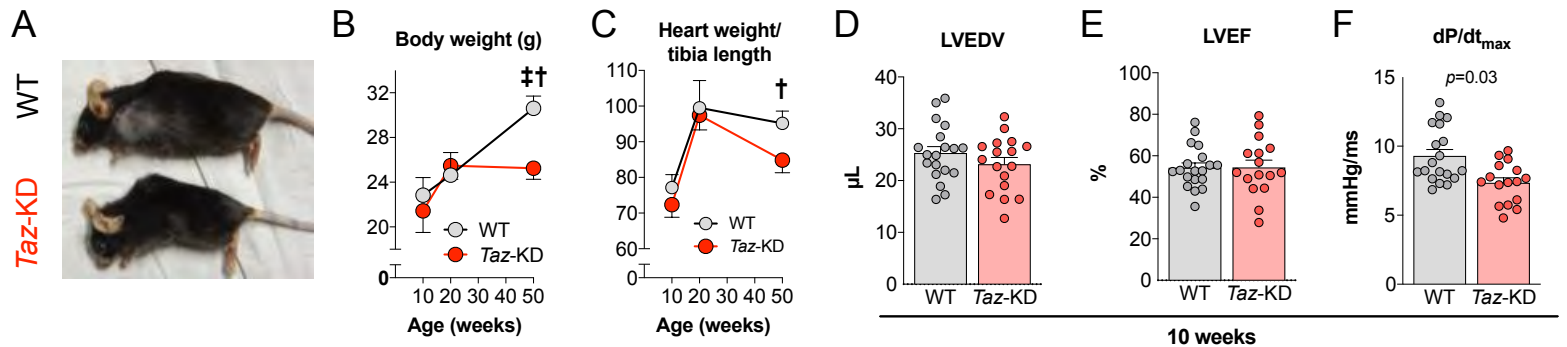
*, **, ***, ****, *****: $p < 0.05$, $p < 0.01$, $p < 0.001$, $p < 0.0001$ with Bonferroni post-test.

§ $p = 0.0011$ within *Taz*-KD + CGP by Dunnett's multiple comparison test between baseline and Dobutamine

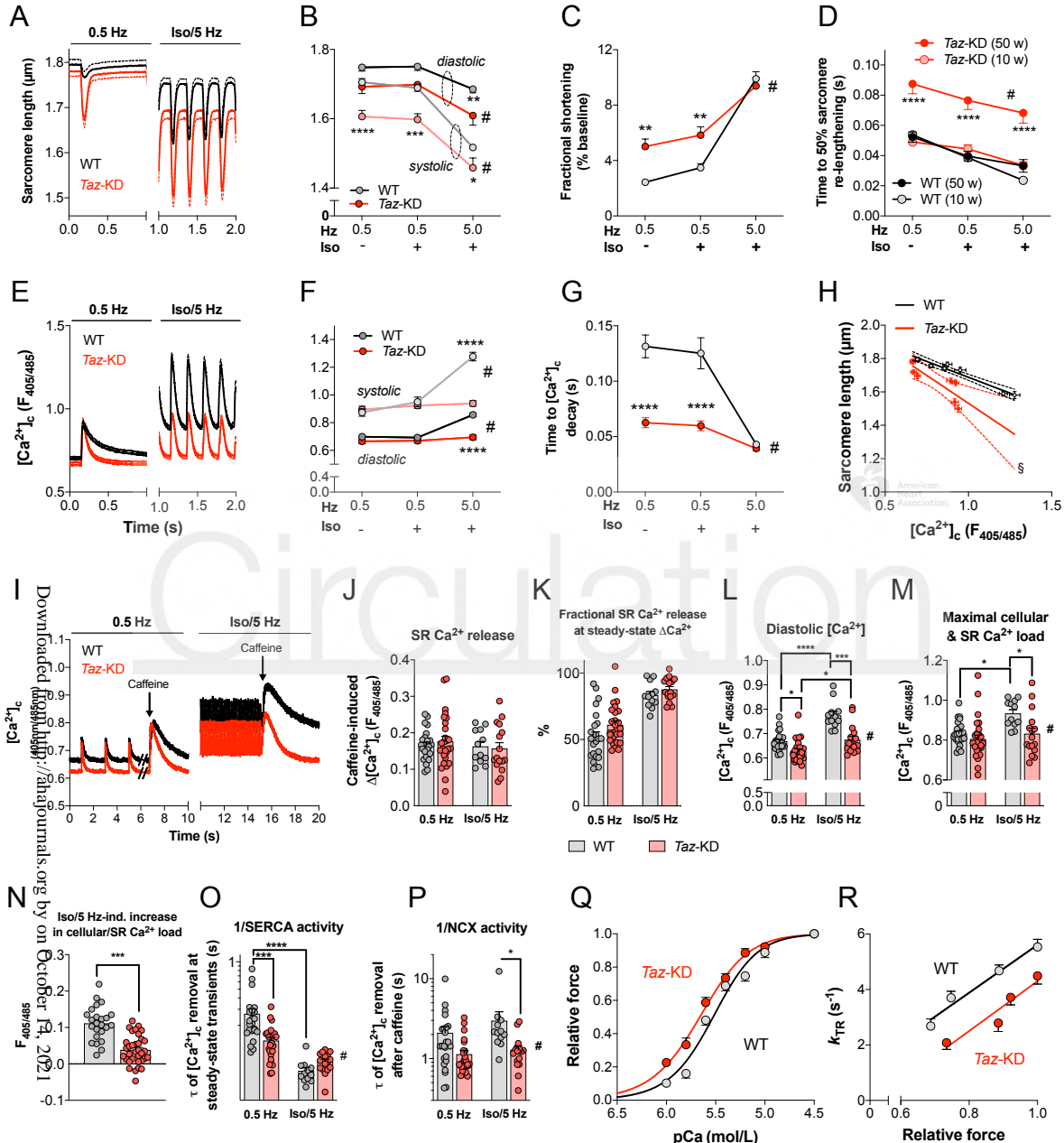
Figure 8. Mechano-Energetic Uncoupling in Cardiac Myocytes of Tafazzin-Deficient Mice

Increased Ca^{2+} affinity of myofilaments cause diastolic dysfunction which is partly compensated by pre-activated activity of sarcoplasmic reticulum Ca^{2+} ATPase (SERCA). Both processes impose an extra energetic burden on mitochondria and limit the contractile reserve during β -adrenergic stimulation and/or increased stimulation frequency in the presence of mechanical preload.

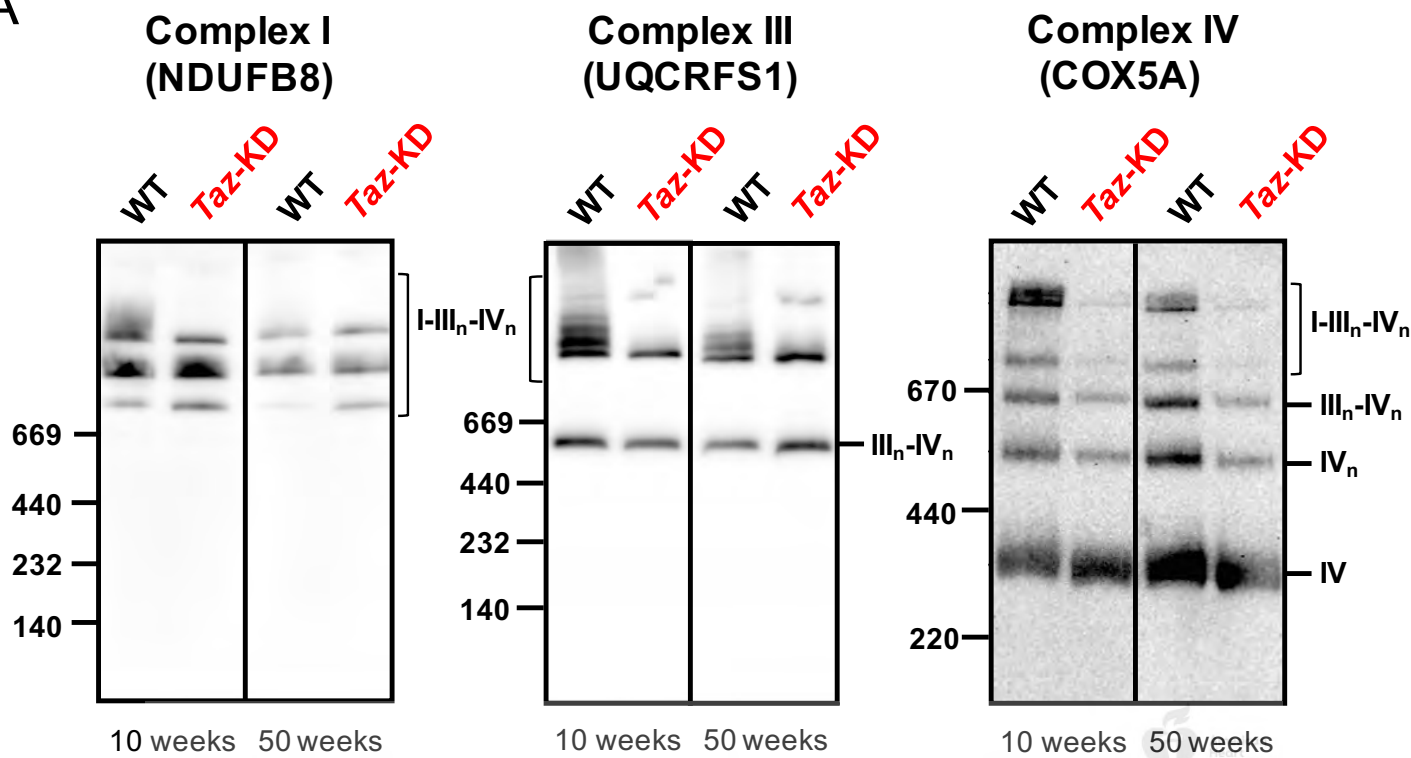
Abbreviations: ADP, adenosine diphosphate; ATP, adenosine triphosphate; CaMKII, Ca^{2+} /calmodulin-dependent protein kinase II; ETC, electron transport chain; MCU, mitochondrial Ca^{2+} uniporter; P, phosphorylation; PKA, protein kinase A; PLN, phospholamban.



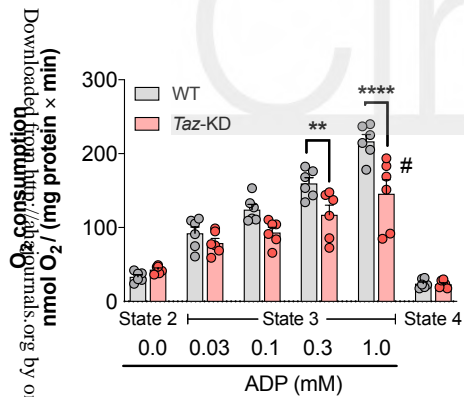
Downloaded from <http://ahajournalsaphapublications.org/> on October 14, 2021



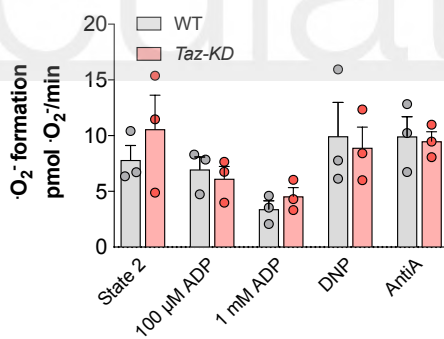
A



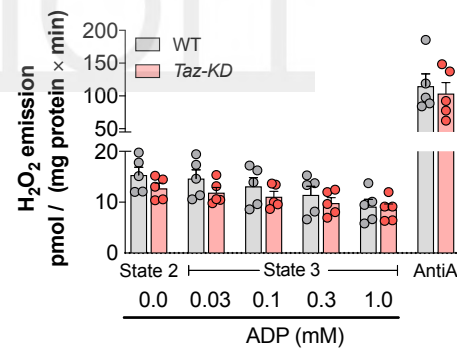
B



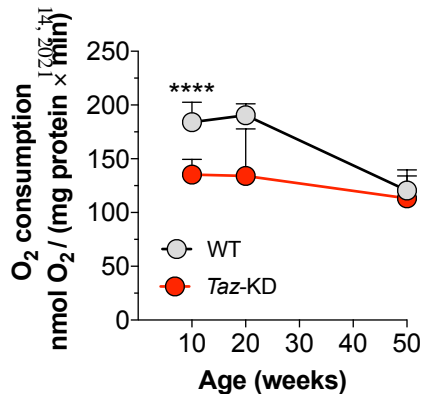
C



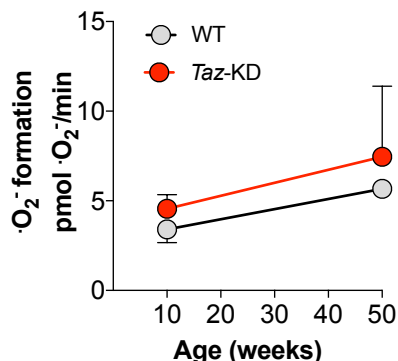
D



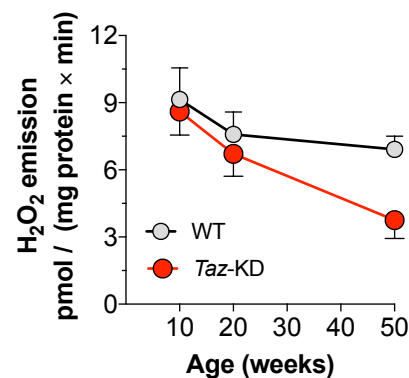
E

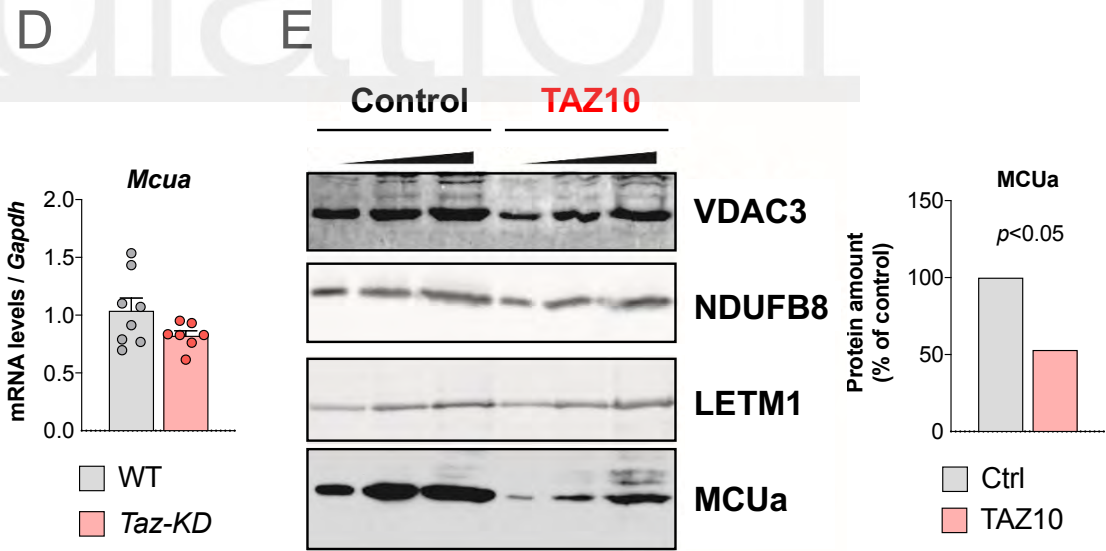
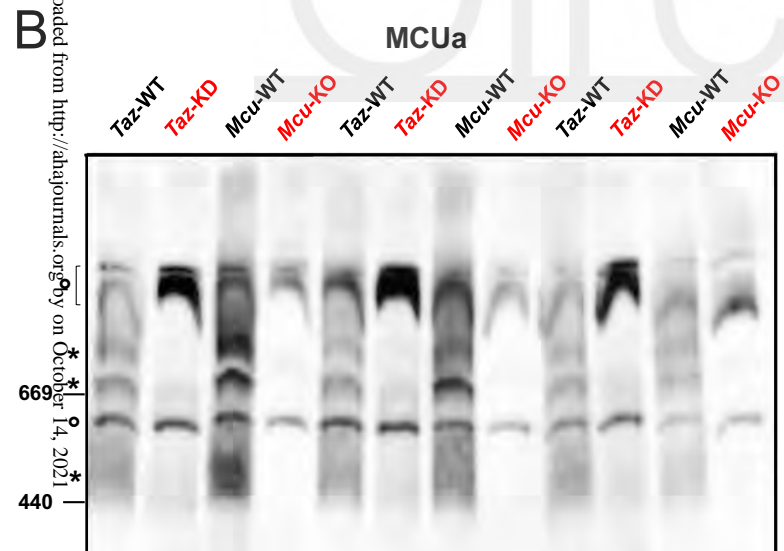
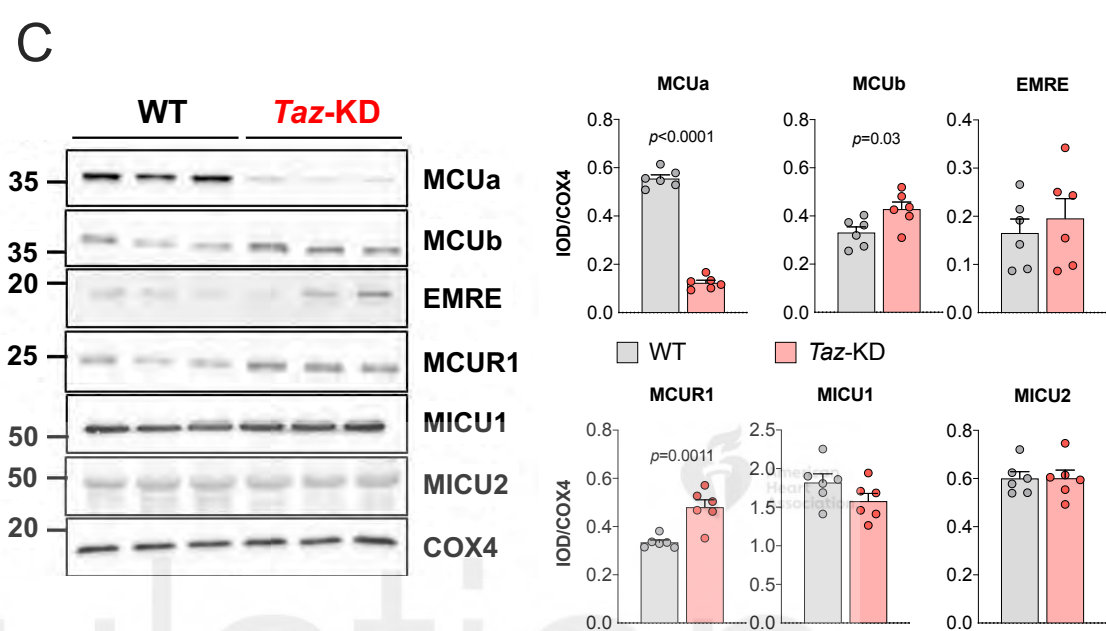
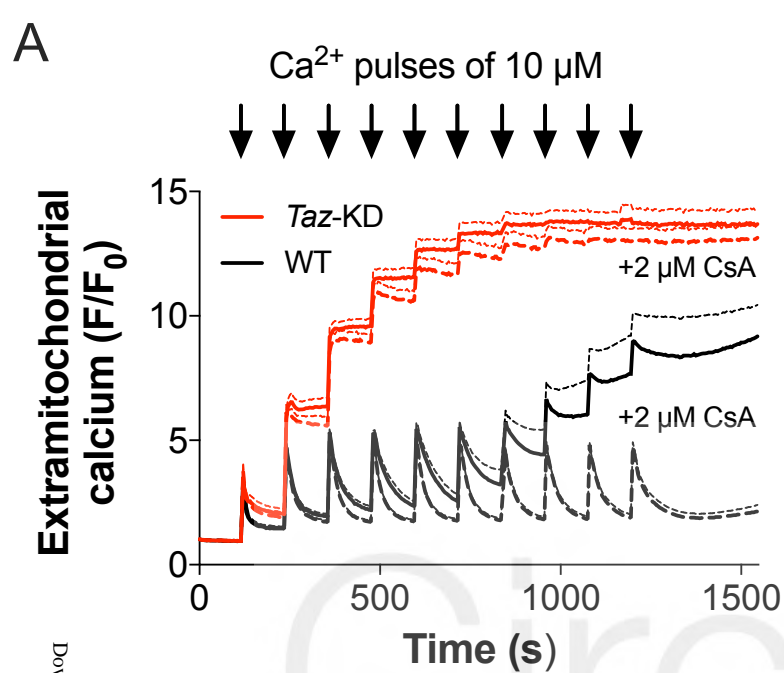


F

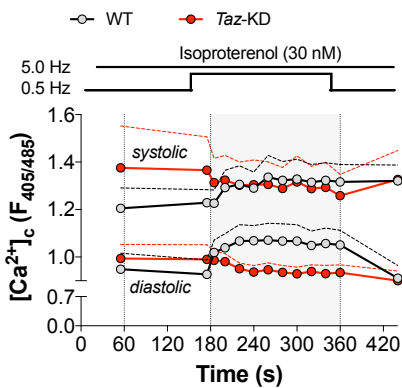


G

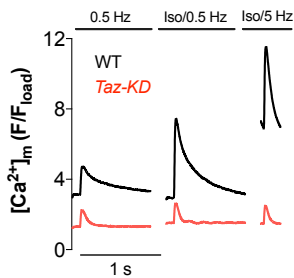




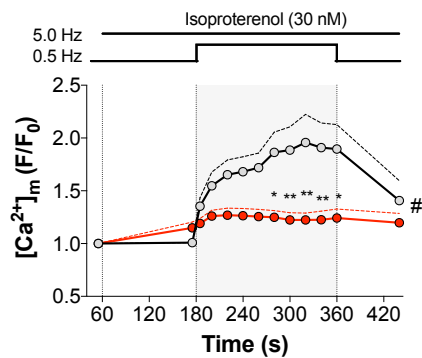
A



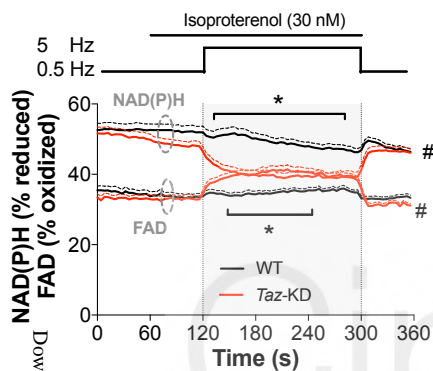
B



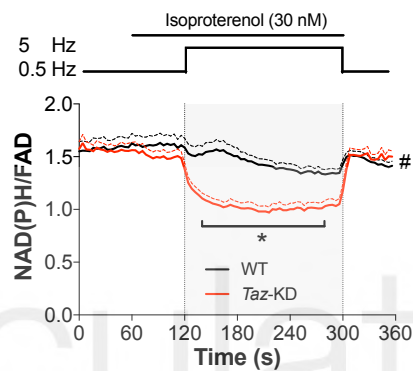
C



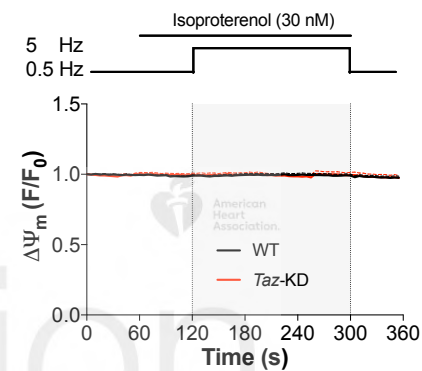
D



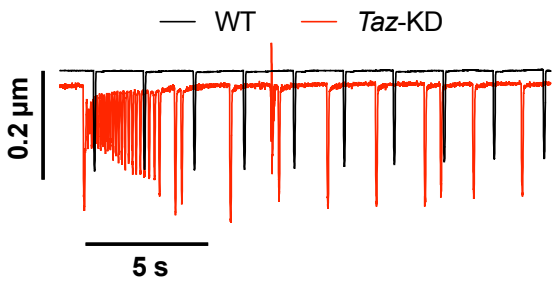
E



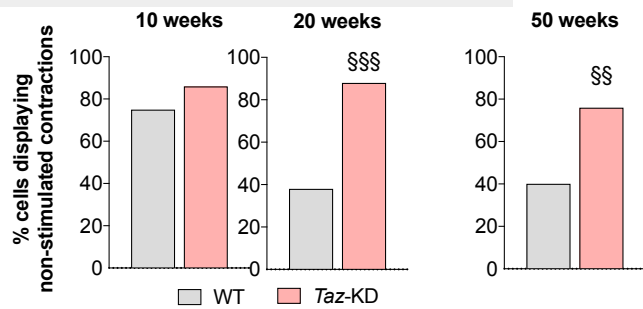
F



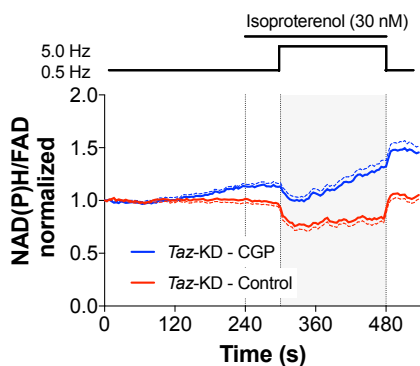
G



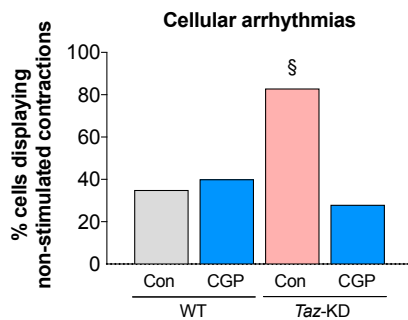
H

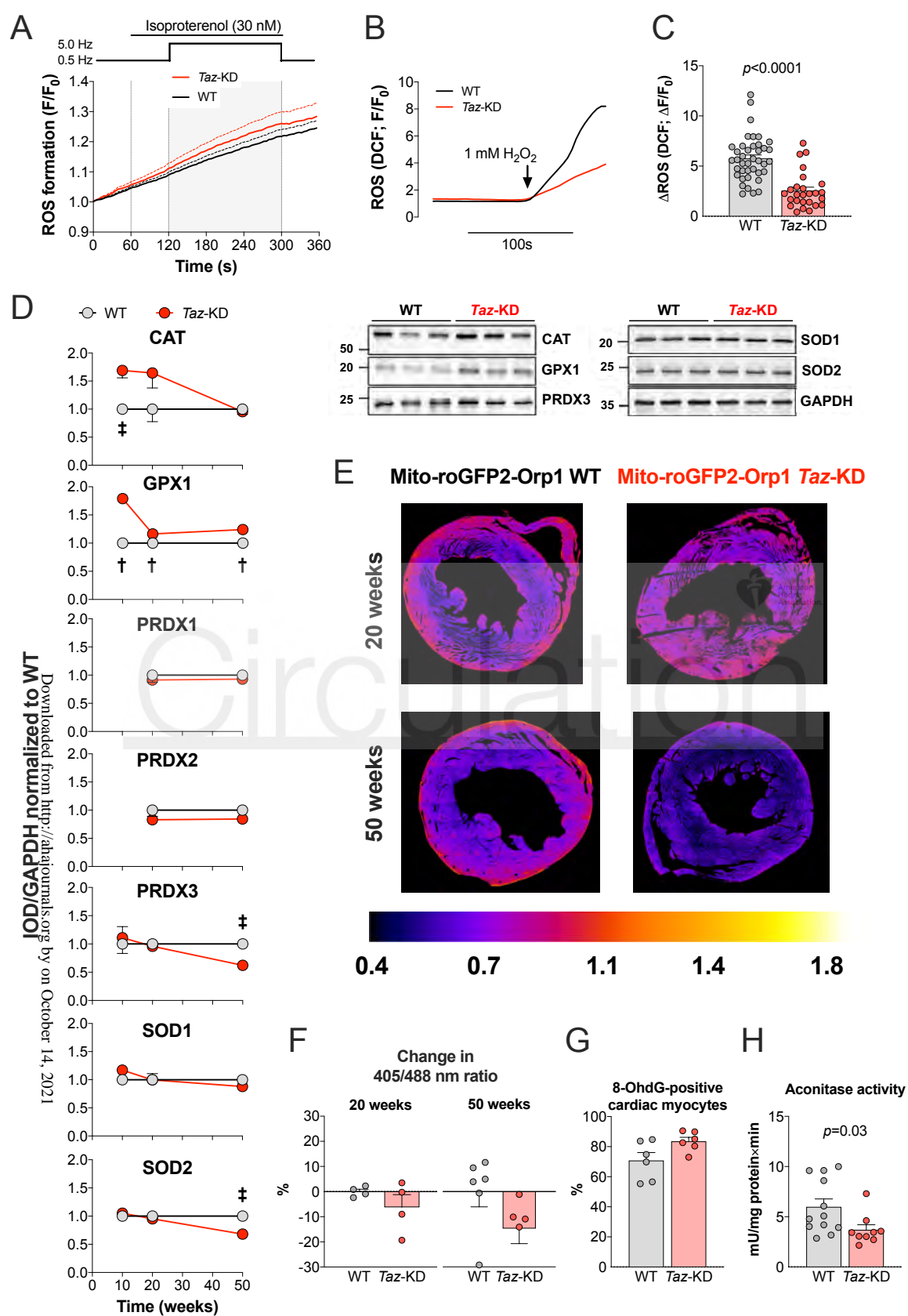


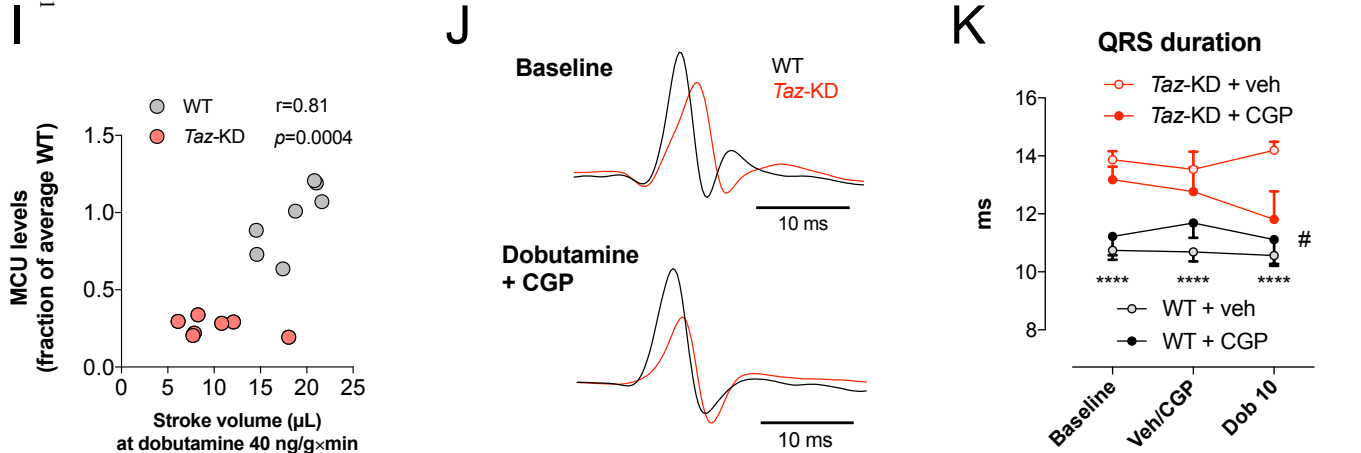
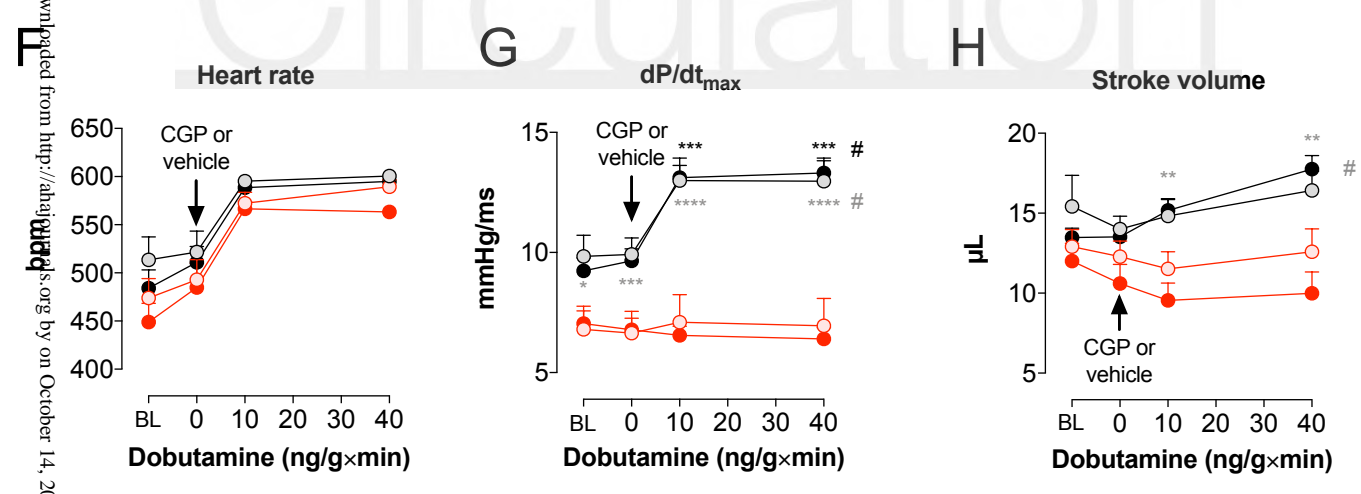
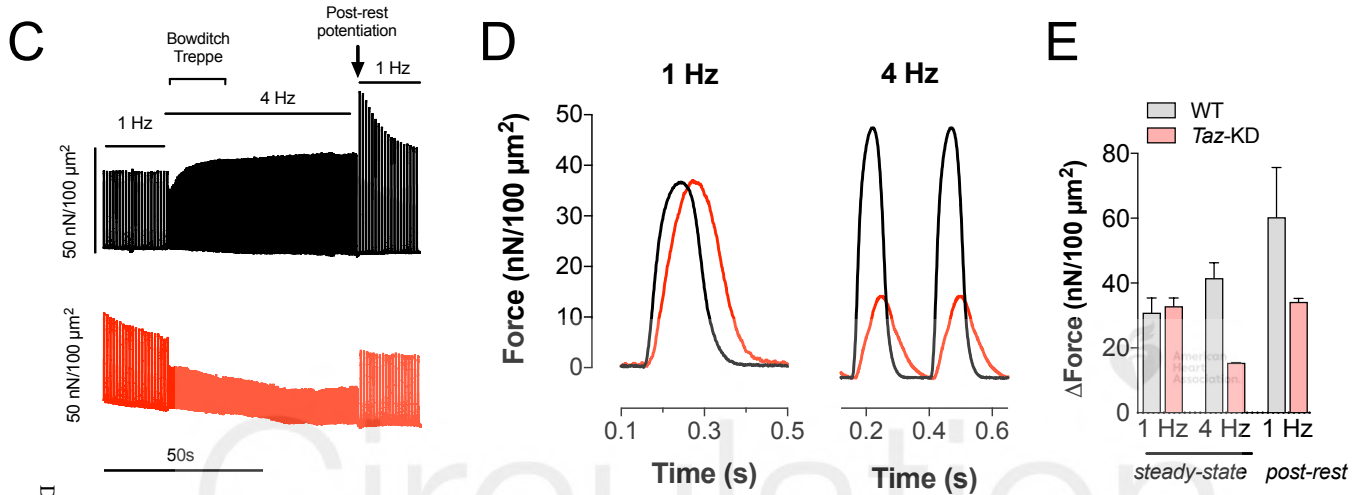
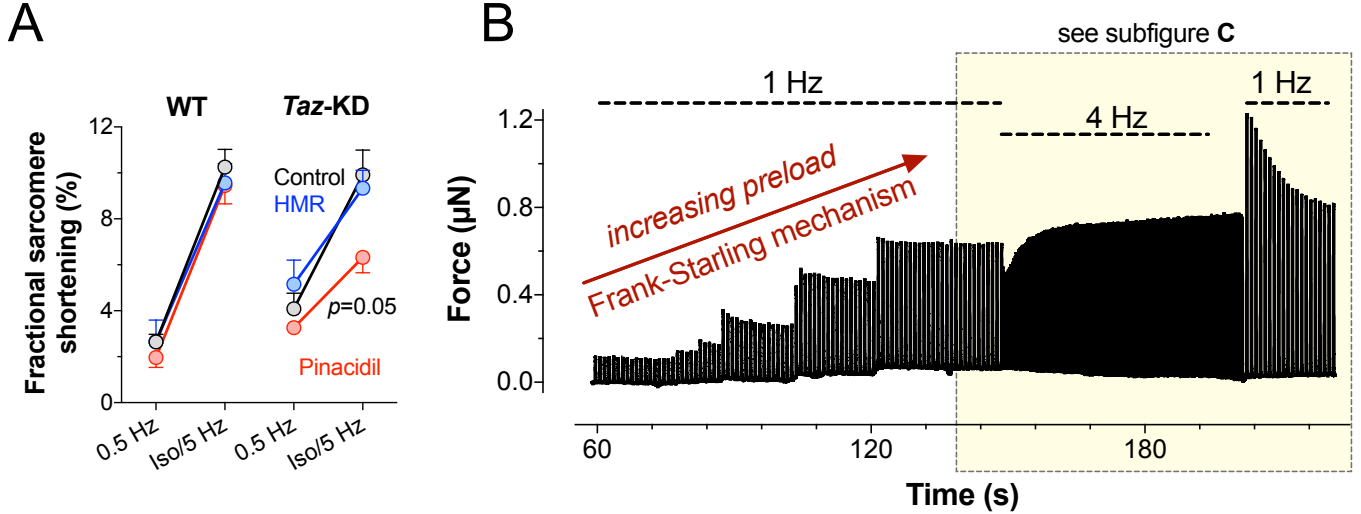
I



J







Downloaded from http://ahajournals.org by on October 14, 2021

Resting conditions

ATP supply ↓

ATP demand ↑

Increased workload

